OXIDATIVE COUPLING OF METHANE TO C_2-HYDROCARBON ON Na_2WO_4-Mn/SiO_2, RHA, OR MULLITE SUPPORTS

INTRODUCTION

In the large natural gas reserves worldwide, methane is the major component of natural gas that appears to be the cheapest and most available carbon source for the gas-based petrochemical industry. Therefore, the development of a process has preceeded for the direct conversion of methane to more valuable chemicals (Ertl *et al*., 1997).

The oxidative coupling of methane (OCM) reaction is a new route to convert methane to C_2-hydrocarbons. It offers a new method for ethylene production reaction (Lunfords, 1995) according to the reaction equation:

$$4CH_4 + 3/2O_2 \longrightarrow C_2H_6 + C_2H_4 + 3H_2O \quad (1)$$

Ethylene is produced from the OCM reaction, which could be used as an important raw material in the production of petrochemicals and ethanol. In the petrochemical process, ethylene is used to produce many commercial products such as plastic, resin, fiber, etc. Also, ethylene could produce ethanol, which used to mix in gasoline process. In the ethanol production, ethanol could be produced via two methods: esterification using of concentrated sulfuric acid following hydrolysis and catalytic hydration over the phosphoric acid catalysts (Faith *et al*., 1957).

Methane is the most stable molecule among any hydrocarbons. The catalytic activation of methane to produce higher hydrocarbons is a difficult process in energy thermodynamics. However, thermodynamics can be overcome by using oxygen molecule as an oxidant to activate methane for production of oxygenated compounds. Moreover, the detailed OCM reaction mechanism is very complicated. Many possible

side reactions can produce carbon monoxide (CO) and carbon dioxide (CO_2) from partial oxidation reactions. When the conditions of the OCM reaction are unsuitable, these reactions can occur because the activation energy of C_2-hydrocarbon formation is higher than CO and CO_2 formation. This causes a drop in conversion of methane, selectivity, and yield of C_2 hydrocarbon (Li, 2003).

A catalyst is a substance that affects not only the rate of the reaction, but it does also affect the equilibrium. Most catalysts used in the OCM reaction consist of metal oxide of which can be separated into three groups: alkali and alkaline earth metal, lanthanide and actinide metal, and transition metal oxide (Li, 2003). These oxides differently affect conversion of methane and selectivity of C_2-hydrocarbon. Therefore, metal oxides are mixed to catalyst compounds for increasing effectiveness of catalysts such as Na_2WO_4-Mn etc. The mixed catalysts give an increase in C_2 selectivity, methane conversion, and stability of the catalyst. However, the perfect catalysts for the reaction should contain high specific surface area and porosity. These properties are found in the oxide supports such as Al_2O_3, TiO_2, MgO, and SiO_2. The properties of supported metal catalyst usually show a strong dependence on both the preparation methods and the thermal (activation) treatments. As usual, the preparation methods of supported-metal catalysts can be categorized into three types: incipient wetness impregnation, deposition-precipitation, and ion exchange (Chang *et al*., 2005).

Rice husk or rice hull is one of the major residues after rice production. It contains 13-29% inorganic component, of which 87-97% is silica (SiO_2) in an amorphous state (Guha *et al*., 1988). Amorphous silica, commonly referred to rice husk ash (RHA), is extracted from rice husk by acid leaching, pyrolysis, and carbon-removing processes. Pure silica with a high specific surface area, high melting point and high porosity can be produced from rice husks (Tsay *et al*., 2001). These properties make the ash a valuable raw material for producing metal-supported catalysts.

In this work, the oxidative coupling of methane to C_2-hydrocarbon is explored using Na_2WO_4-Mn supported on rice husk ash and mullite (RHA-Al_2O_3). The metal and supports are prepared by incipient wetness impregnation method. This technique is frequently adopted in industry due to its simplicity and convenience. The catalytic activity of OCM reaction over the resulting Na_2WO_4-Mn supported on SiO_2, RHA and mullite will be evaluated with the conditions influencing the catalytic activity.

The purposes of this study were:

1. To study the oxidative coupling of methane reaction using Na_2WO_4-Mn catalyst supported on SiO_2, RHA and mullite.

2. To study the effect of the oxidative coupling of methane reaction at various temperatures.

3. To synthesize Na_2WO_4-Mn catalysts supported on SiO_2, RHA and mullite and characterize its properties.

LITERATURE REVIEW

Methane is a main principle component of natural gas located in many different parts of the world. It is an important hydrocarbon resource in the world, which is commercially well known as a very inexpensive and environmentally safe feedstock of fuel supplies (Lunsford, 2000).

1. Definition of methane

Methane is, in a chemical point of view, the smallest molecule in the entire hydrocarbon series, which consists of a central carbon atom with four bonds joining it to four hydrogen atoms. It is not easily transformed into other compounds because of its thermodynamic stability at temperature below 825ºC and because it displays four strong C-H bonds (with energy of 431 kJ) (Moore *et al.*, 1978). Therefore, many researchers are developing processes to enable the conversion of methane to more valuable chemicals and fuels, which include as following (Lunsford, 2000).

1.1 Oxidative coupling of methane (OCM)

The oxidative coupling of methane (OCM) reaction is a new route to convert methane to C_2-hydrocarbons (ethane and ethylene), which are the main products. The conversion of methane is highly affected by the characteristics of catalysts. Lunsford (1995) presented the mechanism of reaction of OCM as following.

A. Methane activation

For metal oxides, it proposed that the activation of methane took place by abstracting hydrogen atom on the oxygen adsorbed species (O_s^-). These species are found by oxide ion vacancy (□) being trapped at O_s^{2-} ions, which are adjacent to O_s^- ions. This process can be expressed as following equations:

$$CH_4 + O_s^- \longrightarrow CH_3^\bullet + OH_s^- \quad (2)$$

$$2OH_s^- \longrightarrow H_2O + O_s^{2-} + \square \quad (3)$$

and $$O_s^{2-} + \square + 1/2O_2 \rightleftharpoons 2O_s^-. \quad (4)$$

Subscripts "s" is an adsorbed species.

The regeneration of O_s^- ion in equation (2) was proposed to occur by equations (3) and (4). The reaction in equation (3) is called dehydroxylation process, which proceeds at high temperature. Also, the reaction in equation 4 requires high temperature, this step includes the dissociation of the O-O bond of an oxidant gas. The reactions in equation (3) and (4) are the rate-determining step in the catalytic production of $CH_3^\bullet$ (methyl radical).

Another controversial mechanistic question concerns the mode of C-H bond activation. According to equation (2), the C-H bond is broken homolytically by the abstraction of a hydrogen atom. By focusing on the basicity of the catalysts and the acidicity of methane, the C-H bond is broken homolytically as indicated in equation (5).

$$CH_4 + M^{n+}\text{-}O^{2-} \longrightarrow CH_3^-\text{-}M^{n+}\text{-}O^{2-}\text{-}H^+ \xrightarrow{O_2} O_2^-\text{-}M^{n+}\text{-}O^{2-}\text{-}H^+ + CH_3^\bullet \quad (5)$$

B. Surface oxygen ions

The activity of the catalysts for OCM reaction may depend on the type of oxygen involved in the reaction. The various types of oxygen presented on the surface of metal oxide catalysts have responsible for the activation of methane, e.g. O^-, O_2^- and O^{2-}, they are formed by the interaction of gaseous oxygen with an oxide surface as following:

$$O_{2(gas)} + e^- \longrightarrow O_2^- \quad (6)$$

$$O_2^- + e^- \longrightarrow 2O^- \quad (7)$$

and $$O^- + e^- \longrightarrow O^{2-}. \quad (8)$$

C. Ethylene formation

Before producing ethylene, the reaction first produces ethane by the oxidative dehydrogenation reaction. Ethane can be formed by coupling reaction of methyl radicals in the gas phase but nearly the surface. Then, ethane is oxidized to form ethylene. The process of ethylene formation is as following:

$$2CH_3^\bullet \longrightarrow C_2H_6, \quad (9)$$

$$C_2H_6 + O^- \longrightarrow C_2H_5^\bullet + HO^- \quad (10)$$

$$C_2H_5^\bullet + O^{2-} \longrightarrow OC_2H_5^- + e^- \quad (11)$$

and $$OC_2H_5^- \longrightarrow C_2H_4 + HO^-. \quad (12)$$

D. Origin and effect of CO_x

In the formation of ethylene by oxidative coupling process, the reaction is limited largely by the undesirable formation of CO and CO_2. Both CO and CO_2 are produced as by products from four possible pathways as following equations:

$$C_2^+ + O_2 \longrightarrow xCO_x \quad (13)$$

$$C_2^+ + xO_s^{2-} \longrightarrow xCO_x \quad (14)$$

$$CH_3^\bullet + O_s^{2-} \longrightarrow OCH_3^- \quad (15)$$

and $CH_3^{\bullet} + O_2 \rightleftharpoons CH_3O_2^{\bullet}$. (16)

In pathway of equation (13), CO and CO_2 are produced from C_2 hydrocarbon with oxygen gas. So the equation (14), C_2 hydrocarbon is reacted with oxygen gas, which is take place on the surface. From $CH_3^{\bullet}$ radical reacted with O_s^{2-} on surface to produce methoxy ions (equation 15), which decompose to CO and CO_2. For equation (16) of a gas-phase reaction between $CH_3^{\bullet}$ radical and O_2 to produce $CH_3O_2^{\bullet}$ radical, the equilibrium reaction may be responsible for CO and CO_2 formation because of the equilibrium $CH_3O_2^{\bullet}$ concentration decrease with increasing temperature and the selectivity of C_2 formation increasing with temperature.

The foregoing mechanisms have been summarized by Lin *et al*. (1988) as shown in Figure 1.

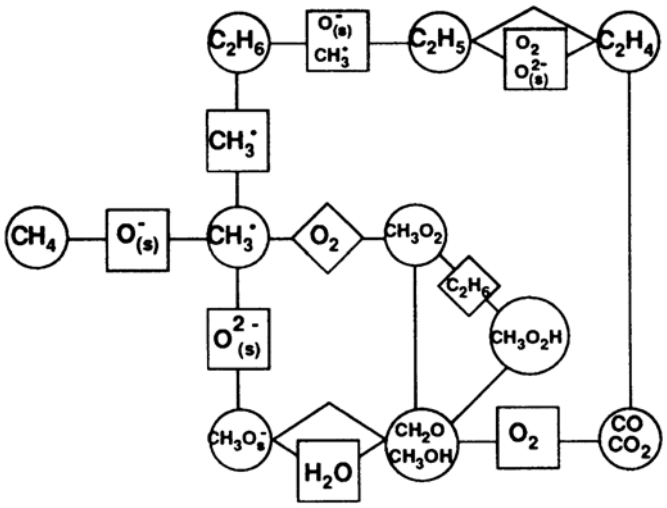

Figure 1 Reaction mechanism for the oxidative coupling of methane.
Source: Lin *et al.* (1988)

1.2 Synthesis gas production from methane

The indirect methods for the utilization of methane require carbon monoxide (CO) and hydrogen (H_2) synthesis gas produced in the appropriate ratios through three principle processes: steam reforming, carbon dioxide reforming, and partial oxidation. Methane reforming reactions are highly endothermic and require extensive heat transfer equipment (Lunsford, 2000).

$$CH_4 + H_2O \longrightarrow CO + 3H_2 \qquad (\Delta H^0_{298\,K} = 206 \text{ kJ/mol}) \qquad (17)$$

$$CH_4 + CO_2 \longrightarrow 2CO + 2H_2 \qquad (\Delta H^0_{298\,K} = 247 \text{ kJ/mol}) \qquad (18)$$

By contrast, partial oxidation is slightly exothermic but requires oxygen or air.

$$CH_4 + 1/2O_2 \longrightarrow CO + 2H_2 \qquad (\Delta H^0_{298\,K} = -35 \text{ kJ/mol}) \qquad (19)$$

1.3 Methane oxidation to methanol and formaldehyde

The greatest potential for a major advance in methane conversion technology is in the discovery of a direct route for the formation of the oxygenate methanol and formaldehyde. The methane monooxygenase (MMO) enzyme, which is able to convert methane to methanol at ambient conditions, is an enticing example of what could be achieved. The enzyme activates O_2 at iron centers with the aid of a reductant known as Nicotinamide adenine dinucleotide (NADH). Using this example, Otsuka *et al*. (1998) showed that $FePO_4$ was an interesting model catalyst for the production of CH_3OH and HCHO when H_2 is added to the CH_4 and O_2 reagents. Presumably, when H_2 reacts with O_2 to form a surface peroxide species, it is responsible for the activation of CH_4 (Lunsford, 2000).

1.4 Conversion to aromatic without an oxidant

Many of the processes described earlier, whether direct or indirect, require the use of oxygen which has a cost that is either equivalent to or greater than the cost of methane. The conversions of methane to aromatic are produced by having methane reacted with hydrogen without an oxidant. Products are such as benzene, toluene and naphthalene.

2. Chemisorption on metals

A belief that the chemisorption of one or more of the reactants is involved in essentially all solid catalyst reaction leading to understand chemisoption phenomena on catalysts and clarify the mechanism of catalytic reaction. The chemisorption of various gases of practical interest has been investigated on many metals. It is found that the strength of chemisorption for some gases and vapors falls in the following sequence (Bond, 1987):

$$O_2 > C_2H_2 > C_2H_4 > CO > H_2 > CO_2 > N_2.$$

The reactivity of metal surface is depended on the chemical nature of the metal. For the nitrogen, this is the most active molecules, whereas oxygen is the easiest molecule to activate. Furthermore, Table 1 showed the ability in chemisorption of various adsorbing species on various kinds of metal groups (Bond, 1987).

Table 1 A classification of metals according to their abilities in chemisorption

Group metals		Gases						
		O_2	C_2H_2	C_2H_4	CO	H_2	CO_2	N_2
A	Ti, Zr, Hf, V, Nb, Ta, Cr, Mo, W, Fe, Ru, Os	+	+	+	+	+	+	+
B_1	Ni, Co	+	+	+	+	+	+	-
B_2	Rh, Pd, Pt, Ir	+	+	+	+	+	-	-
B_3	Mn, Cu	+	+	+	+	±	-	-
C	Al, Au	+	+	+	+	-	-	-
D	Li, Na, K	+	+	-	-	-	-	-
E	Mg, Ag, Zn, Cd, In, Si, Ge, Sn, Pb, As, Sb, Bi	+	-	-	-	-	-	-

(+ means that strong chemisorption occur; ± means that it is weak; - means unobservable.)
Source: Bond (1987)

According to the Table 1, it shows that the metals of class A appearing in group IVB, V, VII and $VIII_1$ of the periodic classification, those of class B_1 are the base metal of group $VIII_2$ and $VIII_3$, while those of class B_2 are the noble metal of these groups. Class B_3 contains two abnormal metals of the first long series. The propensity which shows strong chemisorption is therefore firmly associated with transition metals. These metals have a strong chemisorption of C_2H_4 and O_2, therefore C_2H_4 from the OCM will be oxidized to CO_x (CO_2 and CO). We may be expected that catalyst in OCM from transition metals will not be effective catalysts to produce C_2 hydrocarbons. Consider that all of the most weakly chemisorption metals (class C, D and E) come either before or after the transition series proper. These groups have an ability in chemisorption only of O_2 (C_2H_4 is not involved in OCM), therefore, the active metal cation sites have to absorb the gaseous oxygen at their maximum

capacity. In addition especially class D and E, their capability of forming peroxide and/or superoxide make them the active catalysts in OCM to ethane and ethylene.

3. Diffusion on the surface catalyst

The catalyst is the major concerned subject in the OCM reaction. However, there are many important characteristic of catalysts such as pore and surface area. The overall processes of heterogeneous catalytic reaction are related to pores and surface area of catalysts, which can be broken into the sequence of individual steps as following (Bond, 1989).

3.1 Diffusion (mass transfer) of reactants from the bulk fluid to the surface of the catalyst

3.2 Diffusion of reactant into the catalyst through the catalyst pores

3.3 Adsorption reactants on the catalyst surface

3.4 Reaction of adsorbed on the surface of the catalyst

3.5 Desorption of products from the catalyst surface

3.6 Diffusion of products through the catalyst pores to the surface

3.7 Diffusion of products through the surface to the bulk fluid.

Step A and B are the physical process, where the reactants proceed through the gaseous phase surrounding the solid catalyst to the active sites on the surface. Step C, D, and E are chemical in nature, and may be regarded as jointly constituting the catalytic reaction. Step F and G are the corresponding process for getting products away from the surface.

4. Surface area

This issue concerning the catalyst morphology is discussed for the surface area of the methane oxidative coupling catalysts. The generally reaction of methane was required the large surface area of catalyst, whereas, the oxidative coupling of methane was accepted for low surface area of catalyst (Bond, 1987).

These particular issues of the oxidative coupling catalysts are used by alkali-promoted oxides, which decrease surface area with time on stream. Palermo *et al*. (1998) presented an interesting review on the use of Na-promoted silica in OCM reaction. The resulting of surface area of catalyst was decreased with comparing to the catalyst without alkali component.

Another process related to the loss of the surface area is the effect of sintering or calcinations of catalysts. Studies of the effect of calcinations temperature on the surface area of alkali-promoted catalysts were conducted by Palermo et al. (1998). In the resulting of Na/SiO_2 an example catalyst, the surface area was decreased from 130 m^2g^{-1} to 5 m^2g^{-1} after calcinations at 800ºC.

5. Catalyst

The goal of a catalyst in the OCM reaction is often to maximize C_2 yield by varying catalysts, composition, reagent partial pressure, etc. However, in the economic evaluations, the selectivity becomes important, which is even more important than yield, to obtain a modest value of CH_4 conversion.

The most effective catalysts used in the OCM reaction consist of metal oxide, which can be separated in to three groups.

5.1 The alkali and alkali earth metal oxide

Yamamura *et al*. (1995) studied the OCM reaction over ternary metal oxide catalysts, which consist of Group I, III and V element in the periodic table. The C_2 selectivity was increased but the methane conversion decreased when alkali metal was added to Group III metal. The addition of niobium to a Na/La catalyst increased the catalytic activity as a result of the change of La_2O_3 to La_3NbO_7 but C_2 selectivity decreased remarkably because of the disappearance of new base site. Kondratenko *et al*. (1995) studied the OCM reaction over oxides of alkali earth metal using N_2O or O_2 as an oxidant gas. In comparison of N_2O and O_2, N_2O was shown to be a more

active and a more selective oxidant than O_2 when CH_4 conversion was similar for both oxidants. Taniewski *et al.* (1996) introduced the dilution of the catalyst bed to improve the heat transfer characteristic of a fix-bed catalytic OCM by applying Li/MgO as catalyst and varying the amounts of quartz chips or α-Al_2O_3 as diluents. They found that the dilution with limited amounts of diluents led to the lower and wider hot-spots moved towards the exit from the bed. The dilution of the catalyst bed made the heat removal easier and the catalyst bed was more effectively used. The resulting was confirmed that the presence of quartz stimulated the activation of Li/MgO, whereas a fused α-Al_2O_3 was shown to be almost inactive during several hours. Au *et al.* (1998) presented the catalytic performance of 30 mol% BaO- and 30 mol% BaX_2-Nd_2O_3 catalysts. They found that BaO could enhance the activity of Nd_2O_3, while BaX_2 could improve the C_2 selectivity in the OCM reaction. Path of the halide ions in BaX_2-Nd_2O_3, which had the stability of the halide ions following the order: F^->Cl^->Br^-. BaO-Nd_2O_3 and BaX_2-Nd_2O_3 were generated dioxygen and monooxygen species, both species could activate methane to methyl radical at high temperature. Wang *et al.* (2006) mentioned that the series of $BaCO_3$ (= 0, 2.5, 5, 10, and 15 wt.%)/ La_2O_3 catalysts were prepared by urea combustion method and tested activity in the OCM to C_2 hydrocarbon below 600ºC. The increasing $BaCO_3$ contents from 0 to 15 wt.%, CH_4 conversion and C_2 selectivity were increased from 40.0 to 48.6%. In the characterization, the increasing of $BaCO_3$ content, the specific surface area of catalysts was decreased.

5.2 Lanthanide and actinide metal oxide

Beside corporating lanthanide metal oxide with alkali and alkali earth as mentioned earlier, Traykova *et al.* (1998) presented that a 10% La_2O_3 supported on fused MgO catalyst had been studied for the OCM. The results of X-ray diffraction showed that this catalyst provided active oxygen and vacancies e^- for the surface reaction as shown in equation 15.

$$La_2O_3 \longrightarrow La^{3+}O^{2-}e- + [O] \qquad (20)$$

They found that oxygen conversion was in a transition regime between surface reaction and mass-transport control in the range of 700-825ºC. Oxygen conversion was strictly transport controlled at 850-875ºC while methane reaction rate remained surface control. It was in this oxygen-transport controlled regime at 875ºC that the highest yield of 16.2 mol% C_2 was obtained. Au *et al.* (1998) studied the modified Gd_2O_3 with BaO for the OCM reaction. The results found that the CH_4 conversion, C_2 selectivity and C_2 yield were obtained at 32%, 54%, and 17%, respectively, within 30 mol% BaO/Gd_2O_3 catalyst at 750°C, with the CH_4:O_2:N_2 ratio of 2.5:1.0:11.4 and contact time of 0.6 g s ml^{-1}. Kus *et al.* (2003) showed the catalytic performance in OCM of unmodified pure La_2O_3, Nd_2O_3, ZrO_2 and Nb_2O_5. The results confirmed that the catalytic effectiveness in the OCM process of pure unmodified oxides followed the sequence: $La_2O_3 \geq Nd_2O_3 >> ZrO_2 > Nb_2O_5$. He *et al*. (2004) showed the preparation of nano-CeO_2/ZnO catalysts using a novel combination of homogeneous precipitation and conventional impregnation for the OCM with an oxidant CO_2. The results showed that the conversion of methane over the CeO_2/ZnO nanocatalysts was higher than that obtained from the catalysts prepared by conventional impregnation. With an increase in the amount of the doped ZnO in the nanocatalysts, the conversion of methane decreased while the selectivity of C_2 increased.

5.3 Transition metal oxide

The oxide of the transition metals are normally effective alone only as catalysts for nonselective oxidation. However, when supported or promoted, especially with alkali metal, significant activity for the OCM has been achieved. For example, Gong *et al.* (1995) studied the effect of Li, La, Mn and W added to TiO_2 on the catalytic performance for the OCM reaction. The results showed that Li-La-Mn-W/TiO_2 system exhibited high activity and C_2 hydrocarbon selectivity at 770°C with a gas hourly space velocity (GHSV) of 14400 h^{-1}. The results showed methane conversion of 41.6%, C_2 selectivity of 61.7% and C_2 yield of 25.6%. Murata *et al.* (1998) studied the Li-doped sulfated-zirconia catalysts for the OCM reaction. They found that the catalyst performances were dependent on the sulfate content and calcination temperature. A maximum C_2 yield was attained over the catalysts

containing 6 wt.% sulfate with the calcinations temperature of 923-973 K. The results were closely related to the preparation conditions of sulfated-ZrO_2 as solid super-acids. When the performances of the Li-doped sulfated-ZrO_2 (Li/SZ) catalysts were tested at 1023 K as a function of reaction time, both the C_2 and CO_x selectivity remained constant over the range of 8 h but the CH_4 conversion decreased from 17.5% to 11.9%.

One of the effective catalysts for the OCM reaction is Na_2WO_4-Mn/SiO_2, which are consisting of the alkali and transition metal oxides. This catalyst not only has excellent performance but also is stable for long periods under the reaction (Li, 2003). Many researchers have studied the Na_2WO_4-Mn/SiO_2 and Na_2WO_4-Mn/MgO for the OCM reaction, which are differently catalytic performance at various condition of reaction. Earlier, Wang *et al*. (1995) studied the OCM reaction over oxide-supported Na_2WO_4-Mn catalysts. The activity of Na_2WO_4-Mn/SiO_2 and Na_2WO_4-Mn /MgO was studied using both of a co-feed flow of CH_4/O_2 and a pulse reactor. The CH_4 conversion of 20% and C_2 selectivity of 80% were obtained at 800ºC and 1 atm using a CH_4/O_2 ratio of 8/1. The similar catalytic behaviors of two catalysts suggested that a common active site, consisting of a Na-O-Mn species, might be involved. Na is essential for preventing the complete oxidation of methane, which is required for high selectivity perhaps by isolating the Mn ions in Na_2O/ Na_2O_2/ Na_2CO_3 surface phase. From pulse reaction, the results indicated that the active species were not stable under reaction conditions unless gas phase O_2 was present. Pak and Lunsford (1998) studied the thermal effect during the OCM reaction over Na_2WO_4-Mn supported on SiO_2 and MgO. The result was that the Na_2WO_4-Mn/MgO catalyst underwent deactivation during long times on stream but the Na_2WO_4-Mn/SiO_2 catalyst was stable for periods up to 97 hours. Palermo *et al.* (1998) presented critical influence of the amorphous silica-to-cristobalite phase transition of Na_2WO_4-Mn/SiO_2 catalysts for the OCM reaction. They found that the during calcinations of OCM catalyst precursor, the presence of Na induced crystalline SiO_2 (α- cristobalite) from the amorphous silica. The results indicated that amorphous silica was active but very unselective catalysts, whereas α- cristobalite generated active and highly selective catalysts with respect to the formation of ethylene. When

α-cristobalite was produced from amorphous silica during catalyst synthesis, the resulting material is more effective than when pure α-cristobalite is used as starting material. Kou *et al*. (1998) suggested that the combination of tetrahedral and octahedral metallic cores with different oxidation state from each other was responsible for the catalysis in the OCM reaction and tungsten in a T_d- center was responsible for the activation of methane while the manganese in an O_h-center was responsible mainly for the transformation and transportation of oxygen. As the WO_4 groups disappeared from the surface, tetrahedral coordinated Mn^{2+} sites were formed on the surface probably through the formation of square-planer Mn^{3+}/ Mn^{2+} sites. Thus, T_d $Mn^{2+} \longleftrightarrow D_{4h}$-$Mn^{2+}$/ $Mn^{3+} \longleftrightarrow O_h$-$Mn^{3+}$ began to perform the catalysts continuously. Two tentative structural models involving the possible formation of active oxygen species were considered for the surface ensembles as show in Figure 2.

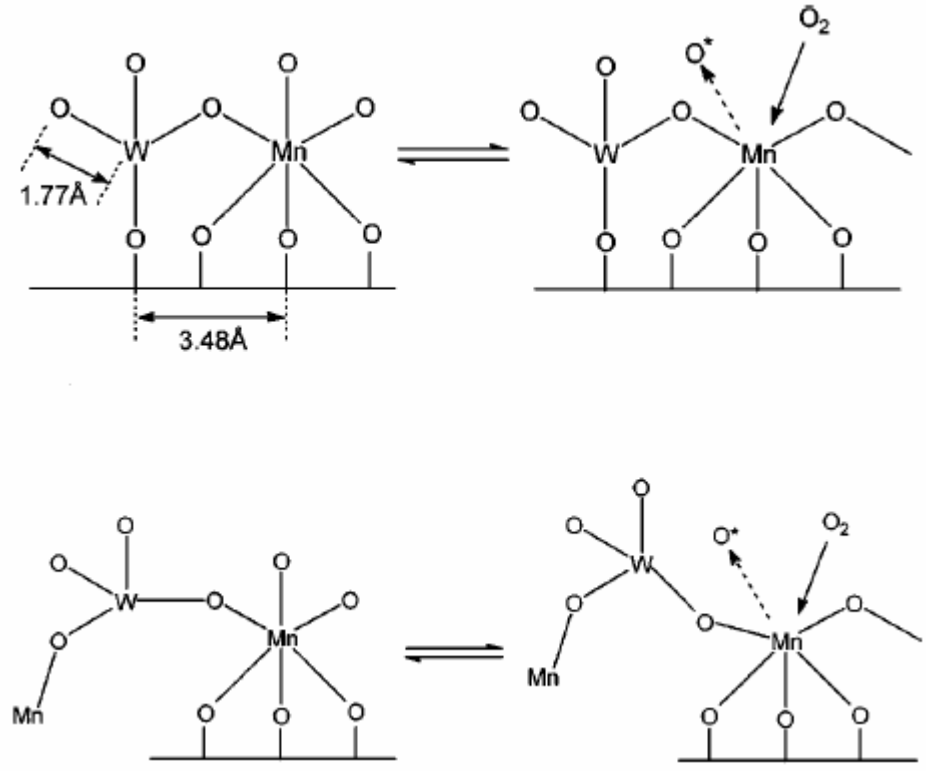

Figure 2 Two tentative models involve the possible formation of active oxygen species (O*).

Focusing on the effect of different metal oxide is a trimetallic system to optimize the catalytic performance. In the study, the series of Na-W-Mn/SiO_2 catalysts were produced by changing the content of Na, W, and Mn. Ji *et al.* (1999) studied the Na-W-Mn/SiO_2 catalysts with different Na content (wt.%) for the OCM reaction. They found that the catalysts with Na content between 0.39 and 2.34 wt% were advantageous to the OCM. Moreover, the addition of Na to the W-Mn/SiO_2 catalyst, W and Mn moved towards the surface of catalyst. Ji *et al.* (2002) studied the catalysis of a series of Na-W-Mn/SiO_2 catalysts with different sodium tungsten and manganese content (wt.%). They found that the catalysts containing Na, W, and Mn between the range of 0.4-2.3, 2.2-8.9, and 0.5-3.0 wt.%, respectively, had high CH_4 conversion and C_2 selectivity in the OCM reaction. They discussed that the active site of the catalysis included Na-O-Mn and Na-O-W species. Tetrahedral WO_4 was first formed with the presence of Na and Mn when the W content was low, when increasing led to the presence of both tetrahedral WO_4 and octahedral WO_6 on the catalyst surface. However, tetrahedral WO_4 was more active and selective for the OCM reaction. From both group of researcher, they concluded that the addition of sodium to the catalyst was believed to bring about with the migration of Mn to the catalyst surface, which was related to the CH_4 conversion and C_2H_4 selectivity.

In the study of the W-Mn/SiO_2 catalysts modified with the metal oxides, Ji *et al.* (2003) studied the activity on the OCM reaction over metal (Li, Na, K, Ba, Ca, Fe, Co, Ni, and Al) promoted W-Mn/SiO_2 catalysts. They found that trimetallic catalysts containing promoted alkali metal showed the best activity of CH_4 conversion and C_2 selectivity. Chou *et al.* (2003) synthesized a new catalyst of SnO_2-doped Na_2WO_4-Mn/SiO_2 by the equal-volume impregnation method for the OCM reaction. The results presented the CH_4 conversion and C_{2+} selectivity of 33.0% and 73.1%, respectively. Moreover, these catalysts provided a large amount of C_3-C_4 hydrocarbons. Hou *et al.* (2006) presented the examination on Mn/SiO_2 and Na salt-modified Mn/SiO_2 catalyst containing different oxo anions, i.e., WO_4^{2-}, MoO_4^{2-}, SO_4^{2-}, PO_4^{3-}, $P_2O_7^{2-}$, CO_3^{2-}, and SiO_3^{2-}. They found that the salt containing MoO_4^{2-}, SO_4^{2-}, PO_4^{3-}, and $P_2O_7^{2-}$ anions were used to producing Mn_2O_3 specie formation with higher reducibility, OCM activity and C_2 selectivity, whereas the basic Na salt of CO_3^{2-}, and

SiO_3^{2-} led to the formation of Mn^{4+} species and to the very low reducibility and OCM activity.

Recently, Wang et al. (2005) synthesized Na_2WO_4-Mn/SiO_2 catalysts by incipient wetness impregnation, mixture slurry, and sol-gel methods and studied the factor influencing the catalytic activity in OCM reaction. They found that the impregnation method could make Na, W and Mn highly distribution on the surface of catalyst. The activity of Na_2WO_4-Mn/SiO_2 catalyst prepared by impregnation and mixture slurry method could be similar, while the sol-gel method exhibited a modest capability to activate oxygen and methane. Stability test showed that the mixture slurry method provided an excellent stability and could alleviate the loss of active components during a 500 h run. Zhang *et al*. (2006) studied the effect of gas space time in gas-phase methane oxidation and in the combination reaction of catalytic OCM over Na_2WO_4-Mn/SiO_2 catalyst. For the gas-phase reaction, methane and oxygen conversions and syngas selectivity increased but the selectivity of C_2 hydrocarbons decreased while the selectivity of carbon dioxide increased slightly with increasing gas space time (t_g) from 6.2 to 7.7 s. However, the concentration of C_2H_4 in the producing mixture was much lower than that of CO and H_2. For the combination reaction, methane conversion and C_2 hydrocarbons selectivity decreased to a minimum with increasing t_g from 3 to 5 s. Zhang *et al*. (2006) presented a new route of methane, converted to H_2, CO and C_2H_4 simultaneously with equal mole ratio; the produced mixture could be used in the synthesis of propanol. Under the optimal reaction condition over Na_2WO_4-Mn/SiO_2 catalyst with CO:H_2: C_2H_4 mole ratio of 1.0:1.0:0.9, the results gave a yield of 11.6% and a selectivity of 68%, while the selectivity to CO_2 was as low as 18.1%.

6. Rice husk ash

Rice husk ash (RHA) is an abundantly available waste material in all rice production obtained after the combustion of the rice husk used as a fuel for parboiling paddy in the rice mills. The rice husk (RH) is one of the by products of rice, which is amenable for value addition. Guha *et al*. (1988) mentioned various uses of RH of

which the most promising included manufacture of industrial chemicals such as silica, sodium silicate, zeolite, activated carbon and refractory materials such as SiC and Si_3N_4. However, the actual utilization in a large scale especially in Thailand is as fertilizer or alternative energy source. In the rice husk or shell of rice seed, the main chemical composition of the rice husk consists of ash, cellulose and lignin. The amount of each composition is different among the various types of rice depending on the paddy, crop year, climatic and geographical condition. The approximate amount of chemical composition is shown in Table 2.

Table 2 Chemical composition of the rice husk

Component	% by weight
Ash	13-29
Lignin	19-47
Cellulose	34-44
Sugar	17-26

Source: Guha *et al*. (1988)

Ash can obtained after combustion of the rice husk, which is consisted of a variety of inorganic matter as shown in Table 3. From Table 3, silica (SiO_2) is the main inorganic component formed in an amorphous state (Guh *et al*., 1981). Amorphous silica is produced with high purity, small particle size and high surface area, which can be used as an adsorbent or catalyst support in fine chemical synthesis. In order to prepare amorphous silica with high purity, rice husk is extracted by chemical leaching, pyrolysis, and carbon-removing or thermal treatment.

Table 3 Composition of rice husk ash

Composition of rice husk ash	Content (%w/w)
SiO_2	91.80
Al_2O_3	0.53
Fe_2O_3	1.54
TiO_2	Trace
P_2O_5	0.89
SO_3	Trace
CaO	0.96
MgO	2.46
Alkalis	1.82

Source: Guha *et al*. (1988)

There are many researches described the silica preparation from rice husk and rice husk ash. Kalapathy *et al*. (2000) presented a simple method for production of pure silica from rice hull ash. A simple method based on alkaline extraction followed by acid precipitation to produce pure silica xerogels from RHA with minimal mineral contaminants. They found that the silica xerogels were produced by heating at 80^{o}C for 12 h having 93% silica and 2.6% moisture. The major impurities of silica produced from RHA at an extraction yield of 91% were Na, K, and Ca. Acid washing prior to extraction resulted in silica with a lower concentration of Ca (<200 ppm). However, final water washing of the xerogel was more effective in producing silica with lower overall mineral content (Na< 200 ppm and K< 400 ppm). Huang *et al.* (2001) obtained silica white from rice husk in a fluidized bed. First, the experiments were carried out in the cold fluidized bed of 90 mm interior diameter (I.D.). The experimental results showed that the ash mixed with a little rice husk could be fluidized when velocity was within the range of 0.18–0.316 m/s. Then, the combustion of rice husk was investigated in the fluidized bed of 84 mm I.D. The results showed that the combustion occurred in the dense zone of the fluidized bed. The ash in the dense zone was easily purified to obtain the SiO_2 powder. Yalcin *et al.*

(2001) investigated the potential and limits of rice husk to prepare relatively pure activated silica. For the activated silica, rice husk samples were submitted to a chemical pre- and post-treatment using HCl, H_2SO_4 and NaOH solutions. Samples were incinerated at 600ºC under static air and flowing atmospheres (air, argon and oxygen). The results showed that the particle size distribution was range from 0.030 to 100 μm. The structure of amorphous silica showed that the specific surface area reached the value of 321 m^2/g, porosity diameter of 0.0045 μm, and specific pore volume of 4.7297 cm^3/g with the high SiO_2 of 99.66%. Kalapathy *et al*. (2002) improved method for production of silica from rice hull ash. In the previously published method, the producing silica xerogel involved dissolving RHA silica with alkali solution to form sodium silicate solution and subsequently forming silica aquagel by adding hydrochloric acid to lower the pH from 11.8 to 7.0 followed by washing and drying aquagel to form xerogel. The results of the silica xerogel had over 4% sodium as a contaminant. They found that an improved method to produce silica xerogel with lower sodium was described by adding silicate solution to pH 1.5 hydrochloric, citric, or oxalic acid solutions until the pH 4.0. The aquagel was washed and dried to form silica xerogel. For comparison silica xerogels were also produced at pH 7.0 by the published method. The results of X-ray photoelectron spectroscopy showed that the silica, sodium, carbon and oxygen content of silica xerogels varied on pH and the type of acid used for the production of these xerogels. Silica xerogels produced by the improved method using citric and oxalic acid had sodium content of 0.52% and 0.22%, respectively. Della *et al.* (2001) developed a procedure to obtain active silica with a high specific surface area from rice husk ash. The relative amount of silica was increased after burning out the carbonaceous materials at different times and temperatures. A 95% silica powder could be produced after heat-treatment at 700ºC for 6 hours. The specific surface area of particles was increased after wet milling from 54 to 81 m^2/g. Feng *et al.* (2004) investigated the properties of rice husk ash using hydrochloric acid pretreatment. They compared the sensitivity of activity of the rice husk ash heated untreated rice husk with the rice husk ash heated hydrochloric acid pretreatment rice husk to burning conditions. The results of heat evolution indicated that the rice husk ash from pretreatment showed the behavior in the increase of cement hydration. The rice husk

ash with pretreatment showed a tendency to shift towards the smaller pore size. Shinohara and Kohyama (2004) studied crystallization of RHA by heating above 900ºC from charcoal rice husk products. They found that the crystalline phases in the two samples were somewhat different. The sample heated in the temperature range of 900 to 1200ºC contained 52–62% cristobalite and 10–17% tridymite but the other sample heated at a comparable temperature above 1100°C contained 46–66% tridymite and 37–16% cristobalite.

7. Mullite

Mullite is one type of aluminosilicate which formula is $Al_2(Al_{2+2x}Si_{2-2x})O_{10-x}$. It is a non-stoichiometric compound with x denoting the number of missing oxygen atoms per average unit cell, varying between 0.17-0.59 (Schneider *et al.*, 1994). The stable compound mullite ($3Al_2O_3.2SiO_2$), which is formed in the Al_2O_3–SiO_2 system is a potential candidate material for advanced structural applications because it has a high melting point, low coefficient of thermal expansion, excellent creep resistance, good chemical stability and high strength at high temperature. This property is suitable for industrial ceramic products such as protection tubes, furnace liners, electrical insulators, catalysts, and refractory bricks (Pak *et al*., 2007). There were many researchers interesting the mullite synthesized. Ribeiro *et al.* (2004) presented the processing of refractory ceramic products by using different shaping technologies, namely, unidirectional dry pressing, extrusion, and slip casting. The results obtained demonstrated that: (i) the flow behavior of the suspensions is strongly affected by the history of the Al-rich sludge and the composition, as well as by the added amount of deflocculant, (ii) the shaping process has a great influence on the final microstructures and material properties, which derive from different degrees of homogeneity and particle packing achieved in the green state. Soluble salts present in the Al-rich sludge create difficulties in achieving proper dispersion and make slip casting products less reliable compared with those consolidated by other shaping techniques. Barea *et al.* (2005) studied the thermal diffusivity of highly porous mullite materials (35–60 vol.% porosity) has been measured up to 1000ºC by the laser flash method. From the point of view of the heat conduction, porous mullite (porosity in the range

~35 to 60 vol.% and pore sizes ~40 μm) behaves as a bi-phase material of voids dispersed in the continuous and dense mullite matrix. The thermal conductivity of materials with porosities ≥45% is almost constant with temperature and ~75% lower than that of the dense mullite. Chakraborty (2005) mentioned reaction between different mixtures of tetra ethyl orthosilicate and aluminum nitrate nonahydrate by DTA technique. The result showed that the two components reacted with the exhibition of an exotherm at 110ºC. During isothermal heating at 80ºC, mixtures showed rise in temperature with vigorous evolution of NO_2 fumes and form gels those on heating to 500ºC form aluminosilicate precursor phase. The composition of it might be to the approximate composition of mullite. Ribeiro *et al.* (2005) synthesized mullite-based refractory ceramic materials from an industrial Al-rich sludge derived from wastewater treatment of aluminium anodizing or surface coating industrial processes, and other low cost raw materials (ball clay, kaolin and diatomite). From the mullitisation process sintered at various temperatures (1250–1650ºC), the performance of the materials at 1650ºC was evaluated to access the microstructural changes occurring under prolonged tests. For dwell times<80 h, a preferential dissolution of the smaller mullite grained in the glassy phase and its partial re-precipitation onto the coarser ones, leading to an overall coarsening of the mullite crystals. For dwell times >80 h, coarse α-alumina and Cr-doped alumina developed at the surface of the specimens, being accompanied by the formation of pores in the vicinity of alumina grains. Montes *et al.* (2007) produced the manufacture of mullite-matrix composites by a colloidal filtration route. Alumina powders were dispersed in a commercial colloidal silica suspension with nanosize silica, which was prepared by ultrasounds probe with citric acid. The results showed that the rheological optimisation allows to obtain low viscosities and to reduce thixotropy and ageing effects. Specimens were obtained by slip casting and sintered to 1550ºC/2 h by using different heating cycles, the best results being obtained with a plateau after the maximum rate of sintering where reaction occurs. Vieira *et al.* (2007) produced mullite from a mixture of raw wastes with slate wastes and aluminium sludges to preparing a mixture with an Al_2O_3:SiO_2 ratio of 2:1. The results of the present study were summarized as follows. The addition of aluminium sludges to slate wastes leads to an increase of mullite content in the sintered product, due to the reaction between

γ-alumina and silica. Sintered products were composites of mullite and γ-alumina dispersed in a glassy phase and presented flexural strengths higher than 100 MPa after sintering temperatures at 1285ºC. She and Ohji (2003) studied the porous mullite ceramics were fabricated by a reaction-bonding technique from a powder mixture of Al_2O_3 and SiC, with graphite particles as the pore-forming agent. They found that the effects of sintering temperature on porosity and strength as well as pore size and surface area were investigated. It had been shown that the strength and pore size increase but the porosity and surface area decrease with the increase in sintering temperature. High surface area of 12.4 m^2g^{-1} was obtained for a 61% porous mullite ceramic, which was observed to have a good thermal-shock resistance to crack propagation.

MATERIALS AND METHODS

Materials

1. Raw materials

Rice husk ash (RHA) obtained from a rice mill in Se-na, Ayutthaya, Thailand, was used as a silica source for catalyst supports and mullite synthesis. Aluminium hydroxide ($Al(OH)_3$) waste from aluminium industry in Thailand was used as an alumina source for mullite synthesis.

2. Reagents

The reagents of sodium hydroxide, carbon dioxide, and hydrochloric acid were used in the preparation of catalyst supports. Sodium hydroxide (NaOH) was purchased from Carlo Erba reagent in Italy, carbon dioxide gas (CO_2) was from Praxair (Thailand), and hydrochloric acid (HCl) was from Labscan in Ireland.

In the active metal oxide over supported of catalyst for OCM reaction, sodium tungstate ($Na_2WO_4.2H_2O$) was purchased from Univar in Australia and manganese nitrate ($Mn(NO_3)_2.4H_2O$) was from Panreac in Spain.

In the OCM reaction, methane gas (99.99%) was purchased from Thai Industrial Gas (TIG) Company in Thailand, oxygen gas (99.6%) and helium gas (99.995%) were from Praxair Company in Thailand.

3. Apparatus

Treated rice husk ash was calcined in a furnace (Chino, KP 1000) at Thailand Institute of Scientific and Technological Research (TISTR). Mullite was sintered in a high temperature electric furnace of King Mongkhut's University of Technology and all catalysts were calcined in a furnace of Lenton Thermal Design. Specific surface

area (S_{BET}) was measured by surface area analyzers of Micromeritic (ASAP 2020) and Quantachrome at TISTR. For the characterization of the catalysts, X-ray diffractometer of Philips (X'Pert) at Material Engineering Department, Kasetsart University, was the equipment used to determine the crystal structure and particle size of metal oxide by using Cu K_α radiation. X-ray photoelectron spectroscope (XPS) using a VG Scientific CLAM 2 energy analyzer at Siam Photon Laboratory, National synchrotron research center was used to determine the binding energy of metal species and near-surface composition (at.%).

The measurement of catalytic OCM reaction activity was carried out in a quartz tube fixed bed reactor under the atmospheric pressure. The analysis of the products was analyzed by a Shimadzu gas chromatograph (GC-14B) at Product Development Technology for Business Division of Kasetsart Agriculture and Agro-Industrial Product Improvement Institute (KAPI) equipped with thermal conductivity detector (TCD) by using WG-100 column and a Hewlett-Packard gas chromatograph (HP-5890) with flame ionization detector (FID) by using DVB-Plot capillary column.

Methods

1. Supported catalyst Preparation

1.1 Silica powder extraction

Silica was extracted from rice husk ash by sodium hydroxide (NaOH). The procedure was described in Figure 3. After the rice husk ash was dried in the oven at 105ºC for 24 hours, it was crushed with ceramic mortar to fine powder. The fine powder was dissolved in NaOH to sodium silicate solution (Na_2SiO_3). Then, the CO_2 gas was passed into the sodium silicate solution to form silica gel. The silica gel was washed with distilled water until neutralized. The gel was dried in the oven at 105ºC for 24 hours to get silica (SiO_2) powder.

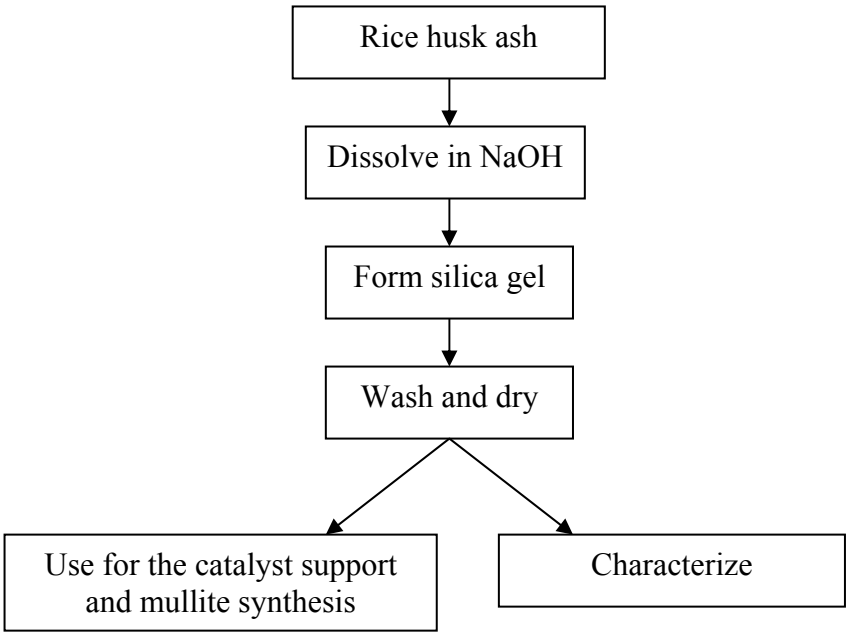

Figure 3 Flowchart for silica powder extraction.

1.2 Rice husk ash treatment

The RHA support could be prepared by starting with 1 and 3M hydrochloric acid (HCl), which was added to RHA waste and stirred at room temperature for 2 hours. The treated RHA was collected by filtration and washed with distilled water until the filtrate was neutral. Then, the neutral RHA was dried at 105ºC overnight and calcined at 500ºC for 3 hours of 1M HCl treated-RHA and 900ºC for 3 hours of 1 and 3M HCl treated-RHA with the heating rate of 5.0ºC/minute and hold for 3 hours. The three supports were denoted by RHA_1_500, RHA_1_900 and RHA_3_900, respectively. The schematic of the procedure was shown in Figure 4.

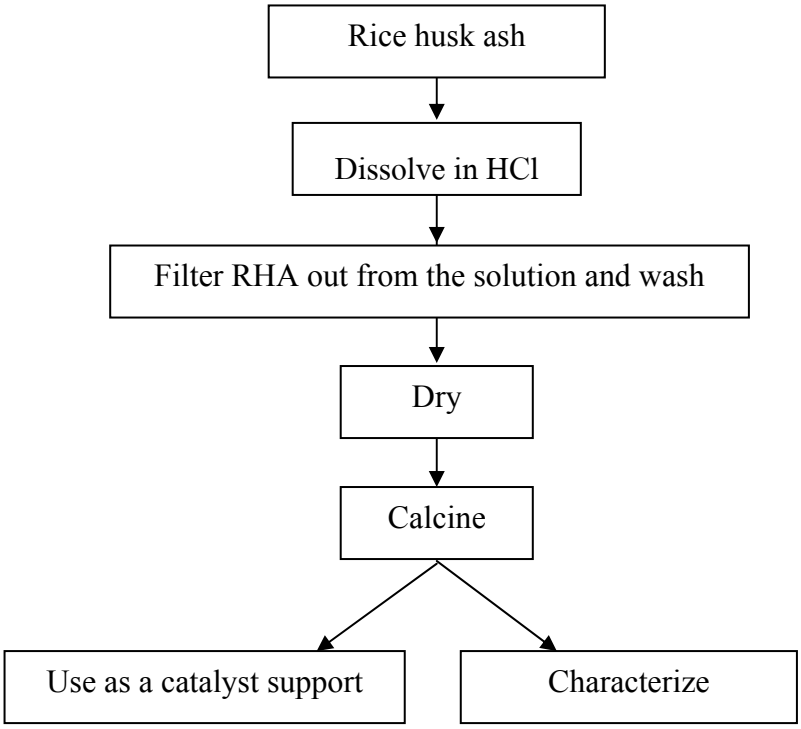

Figure 4 Flowchart of RHA support preparation.

1.3 Mullite sintering

Silica powder (SiO_2) was used as a silica source and aluminium hydroxide ($Al(OH)_3$) was used as an alumina source for mullite synthesis. Prior to use, aluminium hydroxide was purified from industrial aluminium waste, the procedure was described in Figure 5. The impurity was leached out and the remained aluminium hydroxide was washed by distilled water until it became neutral and then dried overnight at 105ºC. The dried aluminium hydroxide was ground to fine powder.

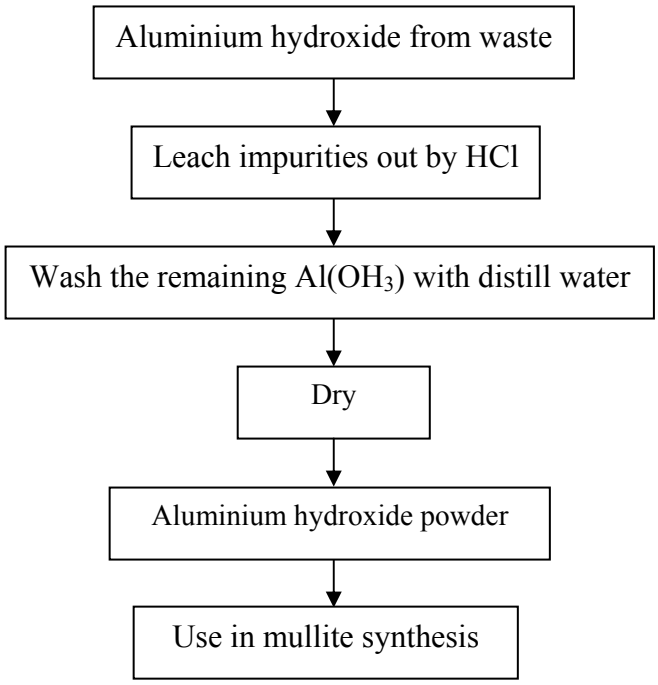

Figure 5 Flowchart for aluminium hydroxide purification

According to the mullite study of Boonpa, (2006) the appropriate percentage of $Al(OH)_3$ and SiO_2 were 66.1 and 33.9 wt%, respectively. Aluminium hydroxide and silica were mixed in pot mill for 24 hours and dried in the oven overnight at 105 ºC. The sintering temperature was varied at 1200, 1300, 1400, and 1500 ºC with the soaking time of 3 hours and the heating rate of 5 ºC/minute in the high temperature furnace, and the four supports were denoted by mullite_1200, mullite_1300, mullite_1400 and mullite_1500. The procedure was described in Figure 6.

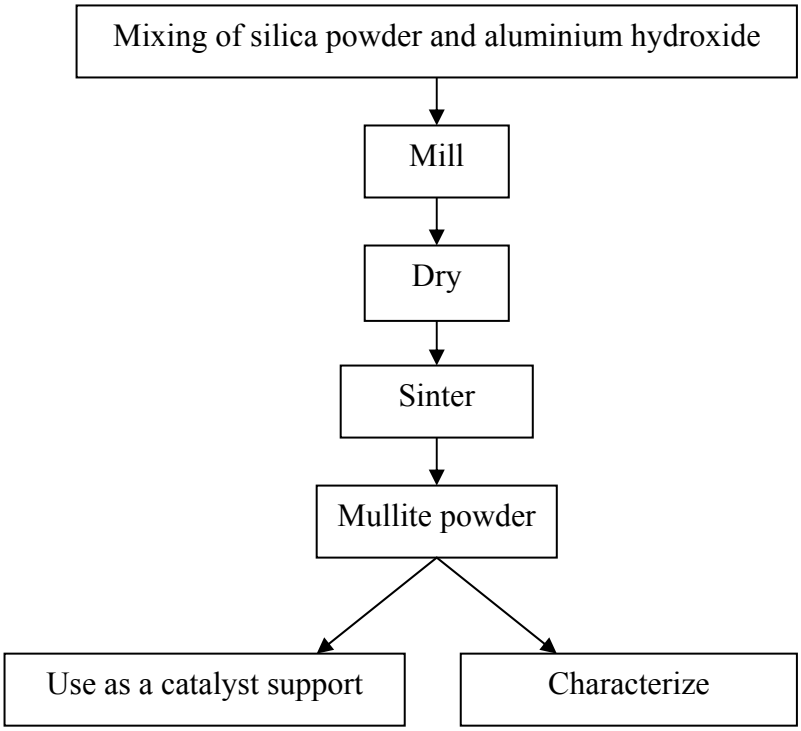

Figure 6 Flowchart for the synthesis of mullite.

2. Catalyst Preparation

Silica, RHA and mullite at various sintering temperatures were used as catalyst supports. The catalysts containing 5 wt% Na_2WO_4 and 2 wt% Mn on supports were prepared by the incipient wetness impregnation method. 10 ml of an aqueous solution containing 0.2807 g of $Na_2WO_4.2H_2O$ and 10 ml of an aqueous solution containing 0.4568 g of $Mn(NO_3)_2.4H_2O$ were added to 2.5 g of each support and stirred the mixture at 80°C. The impregnated sample was dried in an oven overnight at 105°C and calcined in air at 850°C for 6 hours with the heating rate 6ºC/minute. A diagram of the preparation step was shown in Figure 7.

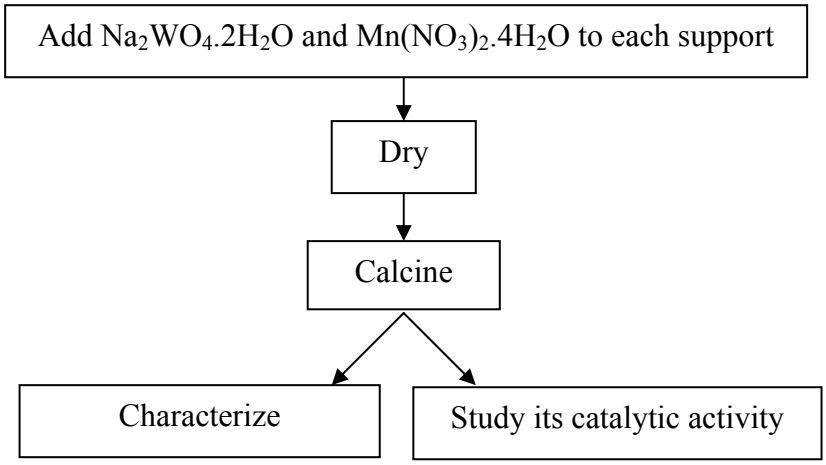

Figure 7 Flowchart of catalyst preparation.

Therefore, three types of catalysts could be obtained namely Na_2WO_4-Mn/SiO_2, Na_2WO_4-Mn/RHA and Na_2WO_4-Mn/mullite.

3. Characterization

3.1 Specific surface area analysis

The specific surface area (S_{BET}) of catalysts and supports was determined by BET (Brunauer Emmett Teller) method. The measurement technique of nitrogen adsorption-desorption method was operated by using relative pressure of nitrogen at 77 K.

3.2 Analysis of phase, crystal structure, and crystallite size

The phases of catalyst, crystal structure, and particle size were analyzed by X-ray diffractometer (XRD) equipped with a CuK_α radiation source at 40 kV and 30 mA and scanning over the range of 2θ = 10-80°.

The mean crystallite size of Na_2WO_4, $MnWO_4$ and Mn_2O_3 particles were calculated from XRD by using the Scherrer's equation (Patterson, 1939).

$$d = K\lambda/\beta\cos\theta \quad (21)$$

K is a particle shape factor constant equal to 0.90; λ is the wavelength of the x-ray radiation employed; β is the full width at half maximum intensity (FWHM); and θ is the angular position of the peak maximum in radian.

3.3 Analysis of the binding energy of metal species and near-surface atomic composition (at.%)

The binding energy of metal species and near-surface compositions (at.%) were analyzed by X-ray photoelectron spectroscope (XPS). Powder samples were pressed on carbon tape mounted on a molybdenum plate. The excitation scan was 300 watts Mg K_α and the pass energy of the analyzer was 30 eV in a step increment of 0.1 eV. The energy scanning range was dependent on each element as shown in Table 4. The binding energies were calibrated using the Si 2p line at 103.4 eV as the reference. Near-surface compositions (at.%) were calculated from peak areas using sensitivity factors provided in the software of the instrument. Data analysis involving peak smoothing, baseline removal, curve fitting, integration, area measurement, and peak marking, was performed on the avantage program.

Table 4 The energy scanning range, the energy step and the number of scan of the investigated elements

Elements	Start (eV)	End (eV)	Step (eV)	No. scan
W	30	50	0.1	10
Al	66	86	0.1	5
Si	94	114	0.1	5
C	275	295	0.1	5
O	525	545	0.1	5
Mn	635	665	0.1	10
Na	1062	1082	0.1	8

4. Catalytic activity test

4.1 Reactor system

The experimental equipments using in this work were designed for heterogeneous reaction using fixed-bed catalyst at atmospheric pressure. The reactant gases, methane, oxygen and helium, were co-fed with the volumetric ratio of 4/1/5 and total flow rate of 100 ml/min into the reactor. Catalyst powder (0.1 g) was placed in the center of the quartz reactor (I.D. = 3.6 mm, length = 500 mm) with quartz wool at both ends of catalyst in the reactor. Thermocouple was put into the center of the reactor to monitor the temperature of the catalyst-bed by electric furnace controller. The flow diagram of the experiment equipments in this work was shown in Figure 8.

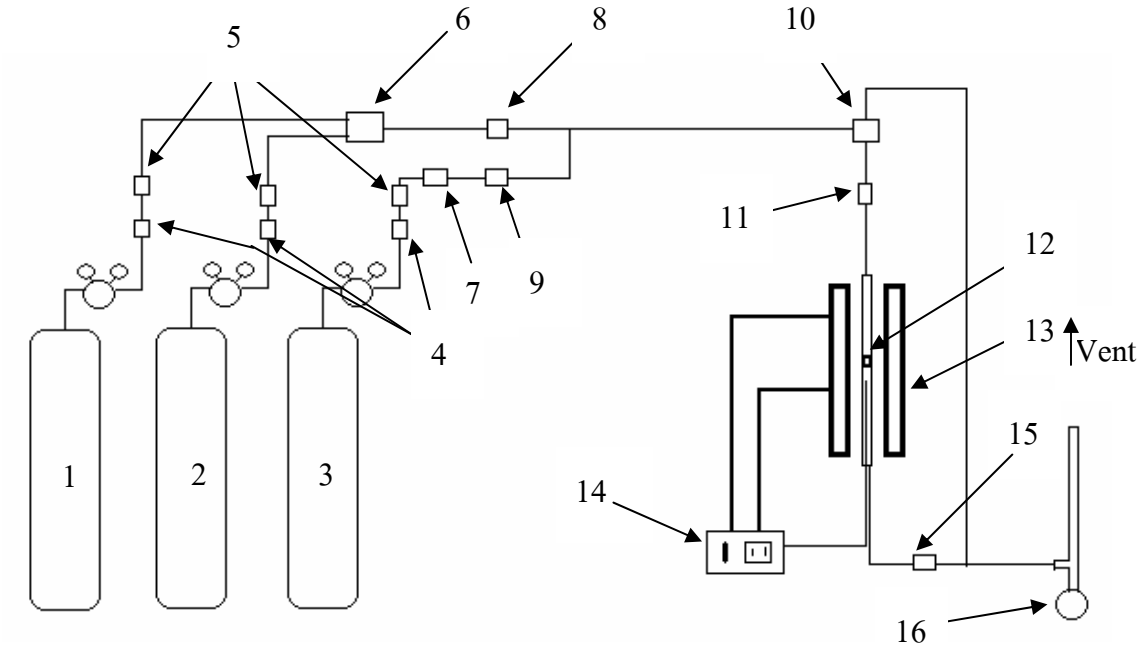

Figure 8 The reaction setup for the OCM reaction.

1. CH_4 gas cylinder	6. rotaflowmeter	11. sampling port
2. O_2 gas cylinder	7. metering valve	12. catalyst bed
3. He gas cylinder	8. check valve (back pressure)	13. electric furnace
4. on-off valve	9. check valve (back pressure)	14. temperature controller
5. gas filter	10. 3-way valve	15. sampling port
		16. bubble flowmeter

4.2 Analysis

The major products for the OCM reaction were analyzed by two equipped gas chromatographs. First, a shimadzu gas chromatograph (GC-14B, Japan) equipped with thermal conductivity detector (TCD) by using WG-100 column with 1/8 inch in diameter and 1.6 m long for the analysis of O_2, CH_4, CO and CO_2; an example of GC chromatogram was shown in Appendix C1. Second, a Hewlett-Packard gas chromatograph (HP-5890, Germany) equipped with flame ionization detector (FID) by using DVB-plot capillary column with 0.32 mm in diameter and 30 m long for the analysis of C_2H_4 and C_2H_6; an example of GC

chromatogram was shown in Appendix C2. The operating condition of gas chromatography was shown in Table 5.

Table 5 The operating condition of gas chromatography

Detector	Parameters	Value
TCD	Carrier gas	He
	Carrier gas flow rate (ml/min)	30
	Column temperature (ºC)	40
	Injection temperature (ºC)	60
	Detector temperature (ºC)	120
	Current (mA)	100
FID	Carrier gas	100
	Carrier gas flow rate (ml/min)	N_2
	Column temperature (ºC)	45
	Injection temperature (ºC)	70
	Detector temperature (ºC)	100

In the catalytic activity testing, the calibration curves of carbon (CO_2, CO and C_2-hydrocarbon) products were constructed as shown in Appendixes C3-C6. The activity of Na_2WO_4-Mn on various supports could be measured by CH_4 conversion using the following calculation:

$$CH_4 \text{ conversion } (\%) = \frac{(\text{Peak area } CH_4)_{in} - (\text{Peak area} CH_4)_{out}}{(\text{Peak area } CH_4)_{in}} \times 100.$$

From the composition (vol.%) of the product stream, C_2 selectivity can be obtained as following:

$$C_2 \text{ selectivity } (\%) = \frac{2 \times \text{vol.\% of all } C_2 \text{ products}}{\text{Total vol.\% of all } C_2 \text{ products}} \times 100.$$

RESULTS AND DISCUSSION

1. Catalysts support characterization

1.1 Rice husk ash

Silica (SiO_2 powder) extracted from rice husk ash and 1M HCl-treated rice husk ash (RHA) calcined at 500ºC, 1M HCl-treated RHA calcined at 900ºC, and 3M HCl-treated RHA calcined at 900ºC with the heating rate of 5ºC/minute and soaking time of 3 hours, which were denoted by RHA_1_500, RHA_1_900 and RHA_3_900, respectively, were characterized by x-ray diffraction in order to verify the phase of silica. XRD patterns of SiO_2 powder and rice husk ash were shown in Figure 9.

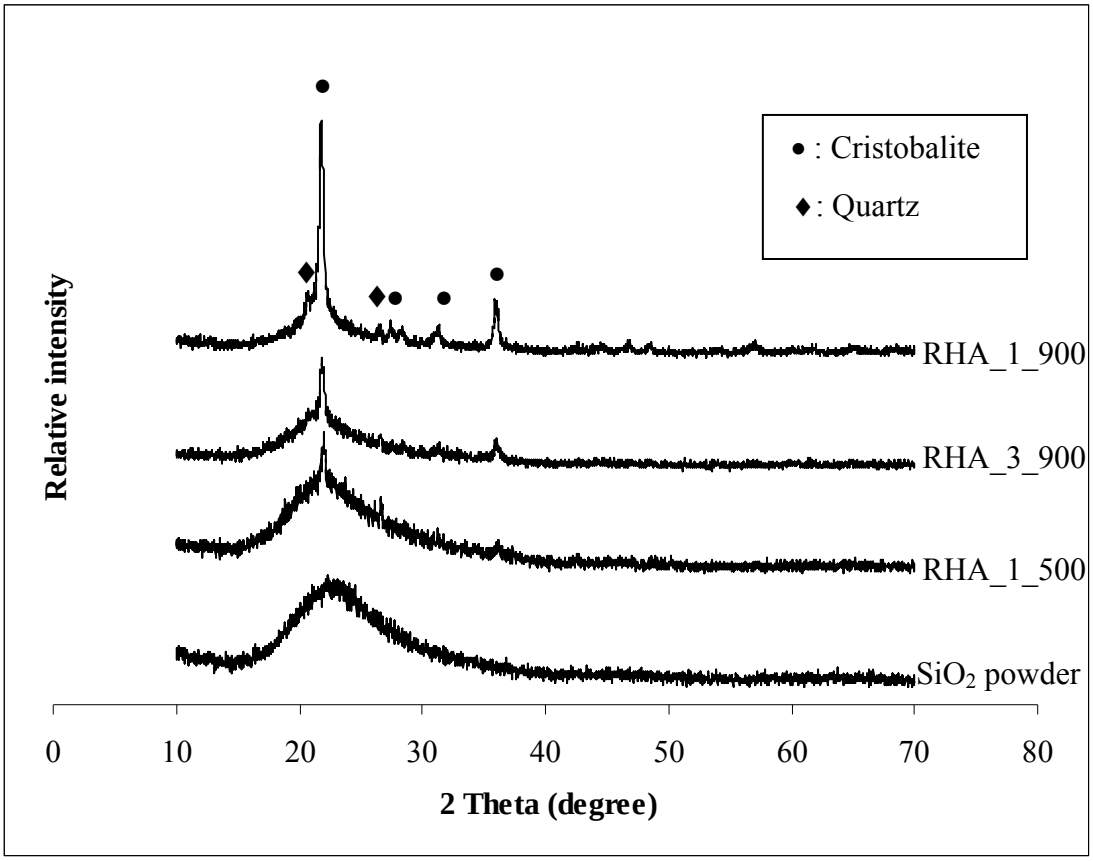

Figure 9 XRD pattern of SiO_2 powder and RHA supports.

To confirm the silica phase, SiO_2 powder showed the blunt peak at 2 theta of 22º, which indicated the phase of silica in amorphous form. When increasing calcination temperature of 1M HCl-treated rice husk ash to 500 and 900ºC, the amorphous silica was undergone to semi-crystalline of quartz and cristobalite as shown in Figure 9 (RHA_1_500) and obtained the highly crystalline quartz and cristobalite phase during calcination at 900ºC as shown in Figure 9 (RHA_1_900). When increasing the concentration of hydrochloric acid from 1M to 3M at the calcination temperature of 900ºC, the amorphous silica phase was transformed to the semi-crystalline phase (RHA_3_900). The presence of quartz and cristobalite were identified by matching with the XRD reference card number 79-1910 (Appendix A1) and 77-1316 (Appendix A2), respectively.

1.2 Mullite

Mullite was prepared by mixing of aluminium hydroxide as an alumina source and silica powder from rice husk ash in the mole ratio of 3:2, respectively. The effect of sintering temperature on mullite synthesis was studied at the temperature of 1200, 1300, 1400 and 1500ºC with the heating rate of 5ºC/minute and the soaking time of 3 hours, and the supports were denoted by mullite_1200, mullite_1300, mullite_1400 and mullite_1500, respectively. Their XRD patterns were shown in Figure 10. The presence of alumina, corundum, cristobalite and mullite were identified by matching with the XRD reference card number 08-0013 (Appendix A3), 83-2080 (Appendix A4), 82-0512 (Appendix A5) and 79-1455 (Appendix A6), respectively.

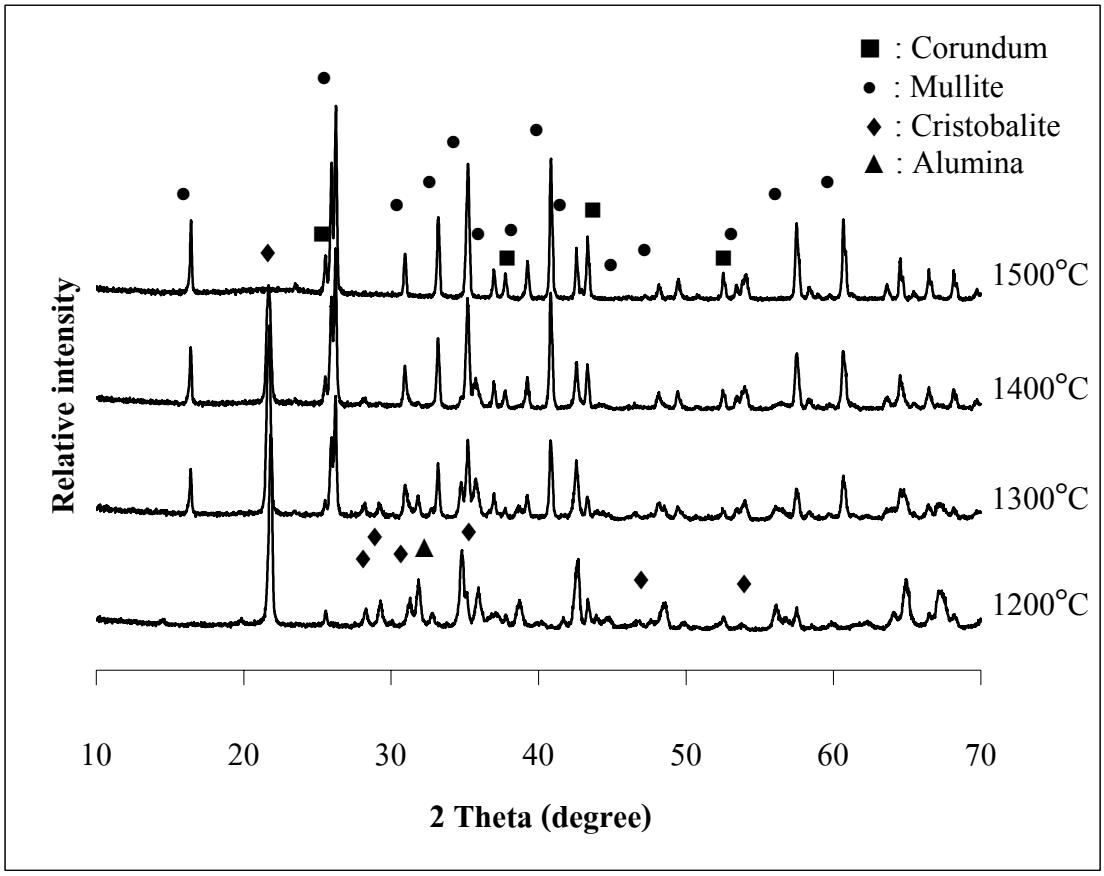

Figure 10 XRD pattern of mullite at various sintering temperature.

At sintering temperature of 1200ºC, the XRD pattern showed the peak of silica in cristobalite phase and alumina phase but there was no major evidence on the mullite formation. The result from Figure 10 showed that after increasing the sintering temperature to 1300ºC, the mullite structure was initially formed, when the increasing sintering temperature to 1400ºC, the intensity of mullite phase was increased whereas the contaminations from the cristobalite phase and the alumina phase were decreased. At the sintering temperature of 1500ºC, the result showed the complete reaction between cristobalite and alumina in order to form mullite phase and the peak of cristobalite phase was disappeared. However, the phase of corundum was increased at the sintering temperature of 1200-1500ºC.

To investigate the specific surface area, silica powder from rice husk ash, rice husk ash treated at various calcination temperatures and concentrations of HCl, and mullite synthesized at various sintering temperatures were measured by the BET method as shown in Table 6.

Table 6 Specific surface area of supports

Support	Specific surface area (m^2/g)
SiO_2 powder	222.80
RHA_1_500	124.80
RHA_1_900	5.19
RHA_3_900	10.98
mullite_1200	11.60
mullite_1300	3.20
mullite_1400	1.53
mullite_1500	0.57

When increasing calcination temperature of 1M HCl-treated rice husk ash from 500ºC (RHA_1_500) to 900ºC (RHA_1_900), the specific surface area was decreased from 124.80 to 5.19 m^2/g due to the complete conversion of semi-crystalline silica to highly crystalline cristobalite phase during the calcination at higher temperature as shown in Figure 9. When increasing the concentration of hydrochloric acid from 1M (RHA_1_900) to 3M (RHA_3_900), the specific surface area was increased to 10.98 m^2/g because the cristobalite phase of rice husk ash was transformed into the semi-crystalline phase because the more concentrated acid had higher ability to dissolve the impurity in RHA and gave the less dense structure as shown in Figure 9. From the mullite synthesis at the calcinations temperature of 1200 and 1300ºC, the specific surface area was suddenly decreased from 11.60 to 3.20 m^2/g, respectively, due to the phase transition from cristobalite and corundum to mullite phase. The mullite synthesis at the calcinations temperature of 1400 and 1500ºC, the specific surface area was obtained 1.53 and 0.57 m^2/g, respectively.

2. Catalysts characterization

2.1 X-ray diffraction

In order to obtain information on the principle components of catalysts, XRD was used to identify bulk phase composition and crystalline size in each catalyst. The XRD patterns of Na_2WO_4-Mn over SiO_2 powder, RHA_1_500, RHA_1_900 and RHA_3_900 after calcination in air at 850°C with the heating rate 6ºC/minute for 6 hours were shown in Figure 11.

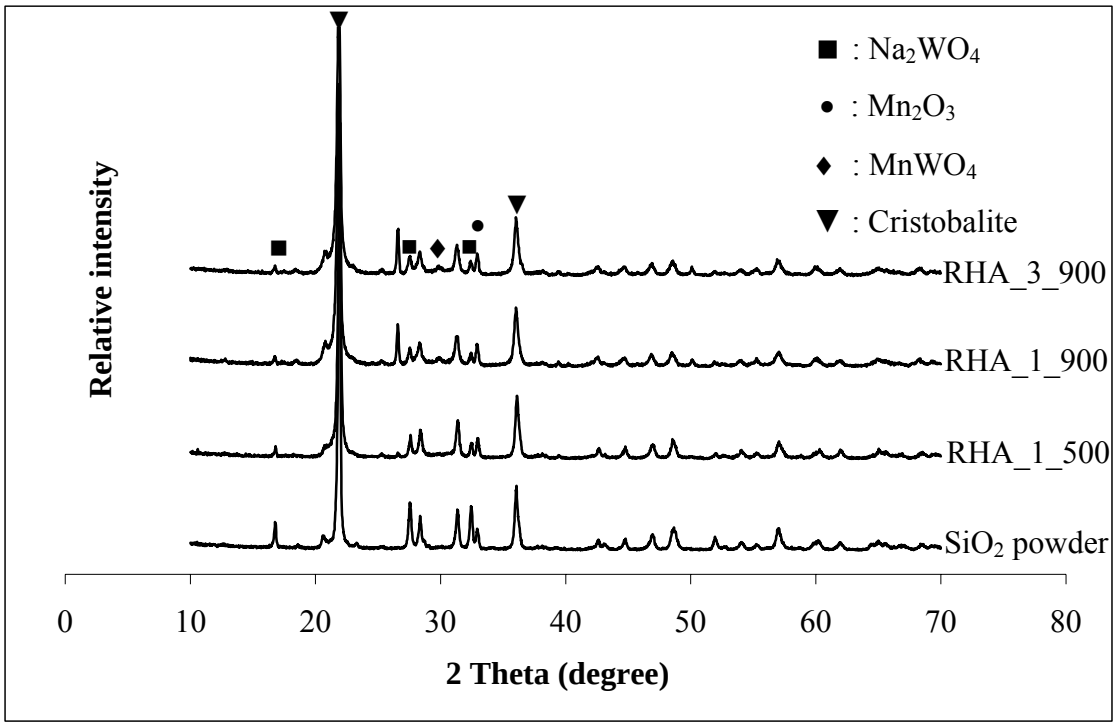

Figure 11 XRD pattern of Na_2WO_4-Mn supported SiO_2 powder and RHA.

It could be seen that the main crystalline phases of the catalysts were Mn_2O_3, Na_2WO_4, and $MnWO_4$. Starting from the amorphous silica phase in various supports, the silica phase was transformed into highly crystalline cristobalite phase during calcination at high temperature. Palermo *et al*., (1998) reported that the phase transition from amorphous silica to cristobalite was important to generate active and highly selective catalysts, especially with respect to formation of ethylene. In the

XRD pattern, the crystalline phase of Na_2WO_4 could be seen at 2θ of 16.80, 27.61 and 32.50. However, the intensity of Na_2WO_4 phase decreased when the supports were changed from SiO_2 powder to RHA_1_500, RHA_1_900 and RHA_3_900, respectively. The Mn_2O_3 peak could be seen at 2θ of 32.92 with similar intensity for all catalysts with different supports. Moreover, the $MnWO_4$ phase was observed for Na_2WO_4-Mn over supported as RHA_1_900 and RHA_3_900. The presence of Na_2WO_4, Mn_2O_3 and $MnWO_4$ were identified by matching with the XRD reference card number 74-2369 (Appendix A7), 73-1826 (Appendix A8) and 72-0478 (Appendix A9), respectively.

The XRD patterns of Na_2WO_4 –Mn over the support of mullite at the sintering temperature of 1200, 1300, 1400 and 1500°C after calcination in air at 850°C with the heating rate 6ºC/minute for 6 hours were shown in Figure 12.

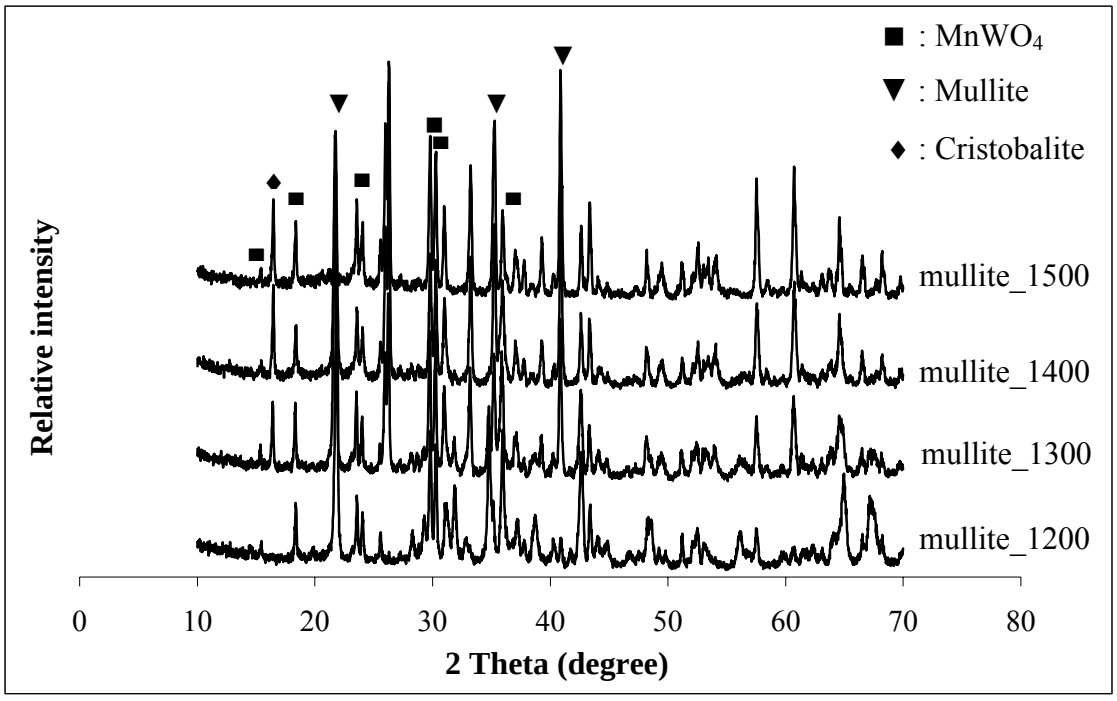

Figure 12 XRD pattern of Na_2WO_4-Mn supported mullite.

It could be seen that the main crystalline phase of the Na_2WO_4-Mn/mullite at various sintering temperatures was $MnWO_4$. The presence of $MnWO_4$ was identified by matching with the XRD reference card number 72-0478 (Appendix A9), 80-0132 (Appendix A10), and 80-0133 (Appendix A11). From literature, Wang *et al.* (1995) stated that the $MnWO_4$ phase could be defined in the term reaction of metal oxide in the catalysts as following:

$$MnO_x + Na_2WO_4 \rightleftharpoons Na_2O + MnWO_4 + 0.5(x-1)O_2. \quad (22)$$

From the results, Na_2O could not be obviously identified because its intensity was interfered by baseline.

From the synthesized catalysts, particles were sieved and the particle size distribution of each catalyst was obtained as shown in Table 7.

Table 7 Particle size distribution of Na_2WO_4-Mn catalyst on various supports.

Particle size (mesh)	Particle size (micron)	wt%		
		SiO_2 powder	RHA_1_500	Mullite_1300
< 100	> 150	8.38	14.95	28.33
100-170	90-150	16.87	25.45	25.73
170-200	75-90	10.89	19.15	14.84
200-270	53-75	23.47	23.75	3.98
270-325	45-53	26.05	12.20	18.39
325-400	38-45	10.85	3.49	4.30
> 400	< 38	3.49	1.00	4.41

Phase identification and crystal size of Na_2WO_4-Mn over supports of silica, HCl-treated RHAs, and mullites were calculated by the Scherrer's formula method (Patterson, 1939) as shown in Table 8.

Table 8 Phase identification and crystal size of the catalysts

Catalysts	Size of crystal phase (nm)[a]		
	Na_2WO_4	Mn_2O_3	$MnWO_4$
Na_2WO_4-Mn/SiO_2 powder	36.69	37.66	
Na_2WO_4-Mn/RHA_1_500	37.94	40.95	
Na_2WO_4-Mn/RHA_1_900	24.91	33.72	9.11
Na_2WO_4-Mn/RHA_3_900	26.73	32.65	8.16
Na_2WO_4-Mn/mullite_1200			43.01
Na_2WO_4-Mn/mullite_1300			47.45
Na_2WO_4-Mn/mullite_1400			37.40
Na_2WO_4-Mn/mullite_1500			44.80

[a] Particle size was estimated using the Scherrer's formula ($d = K\lambda / \beta\cos\theta$).

The phase composition and crystal size of the different catalysts were summarized in Table 7 showing the crystalline phase of Na_2WO_4, Mn_2O_3 and $MnWO_4$. The crystal size of Na_2WO_4 and Mn_2O_3 in Na_2WO_4-Mn/RHA_1_500 was bigger than its of Na_2WO_4-Mn/SiO_2 powder due to the lower specific surface area of RHA_1_500 support. For Na_2WO_4-Mn/RHA_1_900 and Na_2WO_4-Mn/RHA_3_900, the crystal size of Na_2WO_4 and Mn_2O_3 were decreased because of the reaction between Na_2WO_4 and Mn_2O_3 to form $MnWO_4$. For Na_2WO_4-Mn/mullite, the crystal size of $MnWO_4$ was observed without the presence of Na_2WO_4 and Mn_2O_3, the result was agreed with the characterization from XRD as shown in Figure 12.

2.1 BET method of nitrogen adsorption-desorption

Specific surface area of the Na_2WO_4-Mn over supports of silica, HCl-treated RHAs, and mullites was measured by the BET method as shown in Table 9.

Table 9 Specific surface area of catalysts

Catalysts	Specific surface area (m^2/g)
Na_2WO_4-Mn/SiO_2 powder	3.02
Na_2WO_4-Mn/RHA_1_500	1.24
Na_2WO_4-Mn/RHA_1_900	1.94
Na_2WO_4-Mn/RHA_3_900	1.82
Na_2WO_4-Mn/mullite_1200	9.35
Na_2WO_4-Mn/mullite_1300	2.40
Na_2WO_4-Mn/mullite_1400	2.95
Na_2WO_4-Mn/mullite_1500	1.38

To compare the specific surface area between the supports and the prepared catalysts as shown in Table 6 and 9, respectively, the specific surface area of the Na_2WO_4-Mn over the supported silica powder from rice husk ash and the one over HCl-treated rice husk ash treated were dramatically decreased because the amorphous silica was completely transformed into cristobalite after Na_2WO_4 impregnation and calcination at high temperature (Jiang *et al*., 1998). For the Na_2WO_4-Mn over the mullites, the specific surface areas were decreased when using the supports from mullite 1200 and 1300ºC because $MnWO_4$ filled up the surface pores. For the catalysts supported from mullite 1400ºC and 1500ºC, the specific surface area were increased. These indicated that the increase in specific surface area may be expected from the specific surface area of metal oxide aggregates on the surface catalysts. The density of support was increased with the high sintering temperature; the metal oxide was not able to get into pores.

2.2 X-ray photoelectron spectroscopy (XPS)

The XPS photoelectron spectra survey of the various catalysts of Na_2WO_4-Mn/SiO_2 powder, Na_2WO_4-Mn/RHA_1_500 and Na_2WO_4-Mn/mullite_1300 were shown in Figure 13.

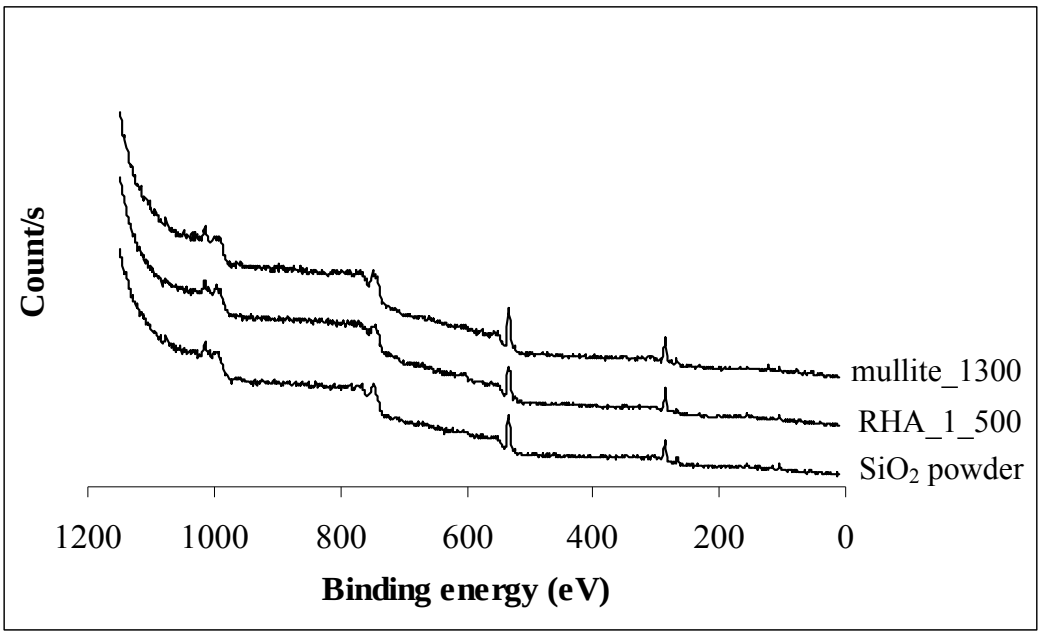

Figure 13 XPS spectra of catalyst.

The XPS photoelectron spectra, binding energy and near-surface composition (at.%) of the species in Na_2WO_4-Mn/SiO_2 powder, Na_2WO_4-Mn/RHA_1_500 and Na_2WO_4-Mn/mullite_1300 were shown in Figures 14-20 and Table 9. Observations of all species were focused on C 1s, O 1s, Si 2p, Na 1s, W 4f, Mn 2p and Al 2p core levels.

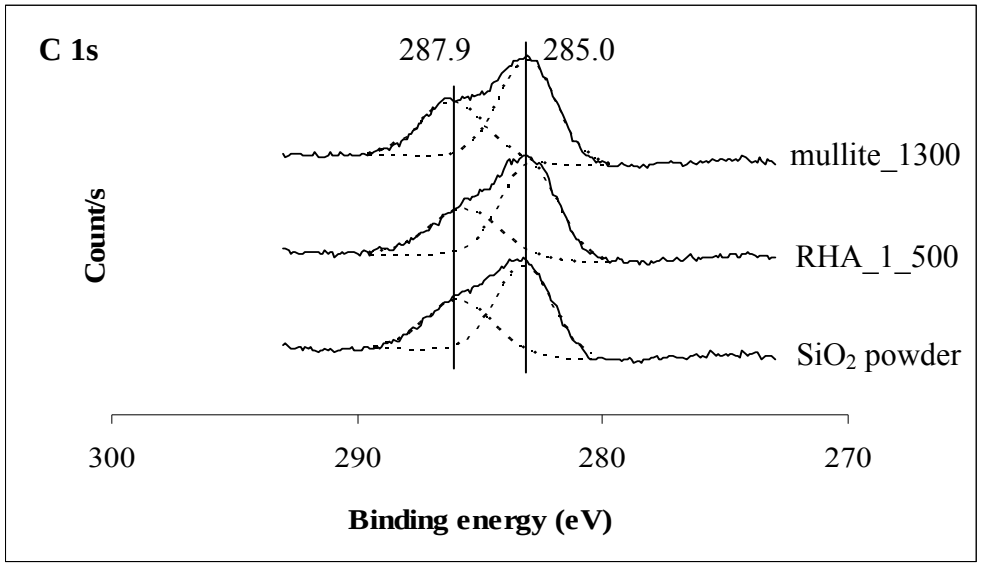

Figure 14 XPS spectra of C 1s region.

In Figure 14, the C 1s binding energies were observed at 285.0 eV for Na_2WO_4-Mn/SiO_2 powder, 285.0 eV for Na_2WO_4-Mn/RHA_1_500, and 285.1 eV for Na_2WO_4-Mn/mullite_1300. The results indicated that the carbon species may be attributed to CO_3^{2-}. The binding energies of carbon species for each catalyst were shifted to 287.9, 287.6 and 288.1 eV, which was presented on the surface of the catalyst (Wang *et al*., 1995).

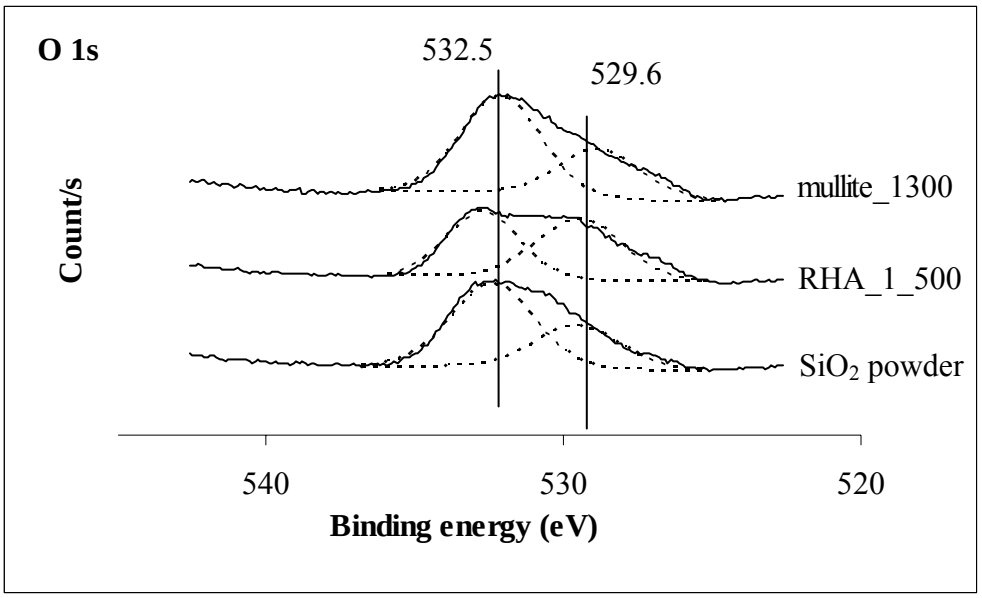

Figure 15 XPS spectra of O 1s region.

From XPS spectra of O 1s, the binding energy around 529.6 eV of Na_2WO_4-Mn over SiO_2 powder, RHA_1_500 and mullite_1300 was corresponded to the O 1s in MO_x (Na_2WO_4, Mn_2O_3 and $MnWO_4$). For the presence of O 1s in SiO_2, the attribution produced a peak at approximate 532 eV (Kou *et al*., 1998).

For the XPS spectra, the binding energy of Si 2p of Na_2WO_4-Mn over SiO_2 powder, RHA_1_500 and mullite_1300 was shown in Figure 16. The Si 2p binding energy of in the range of 103.4 was observed in the catalysts and using as reference peak (Wang *et al*., 2005).

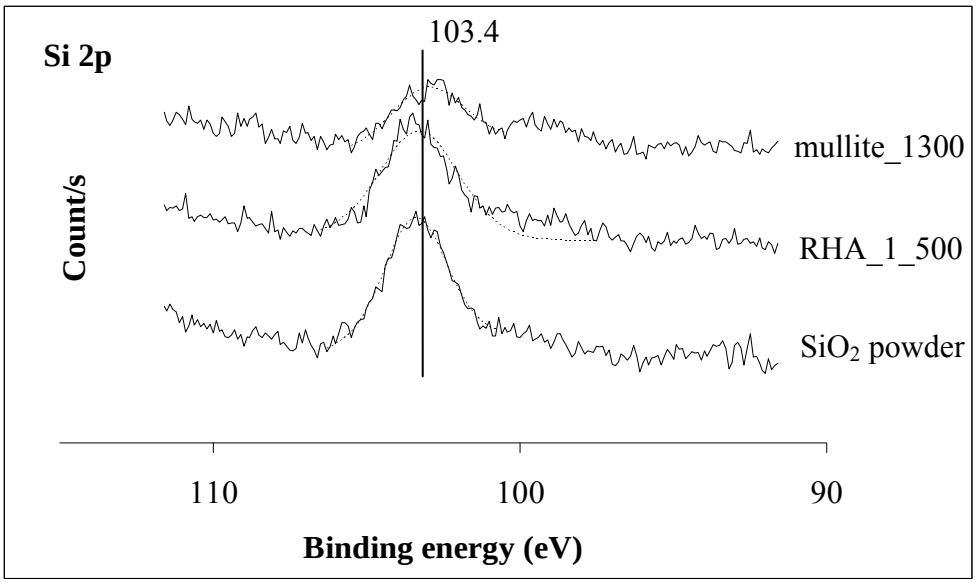

Figure 16 XPS spectra of Si 2p region.

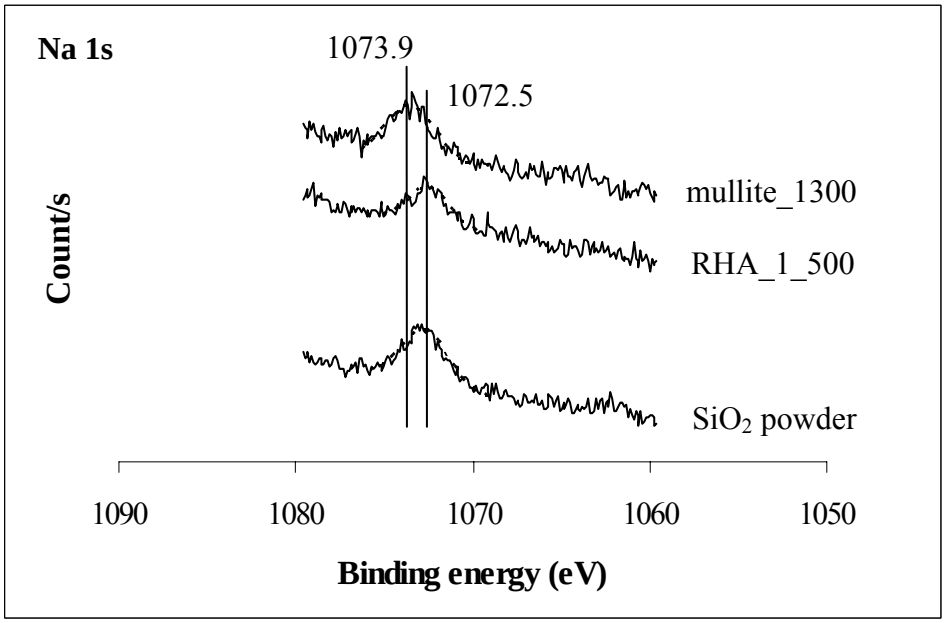

Figure 17 XPS spectra of Na 1s region.

The XPS spectra in the Na 1s were shown in Figure 17. The Na 1s binding energy was attributed to a peak of around 1073.5 eV in Na_2WO_4-Mn over SiO_2 powder and Na_2WO_4-Mn/RHA_1_500. For Na_2WO_4-Mn/mullite_1300, the Na 1s binding energy of 1073.9 was observed, which implied that this spectra was quite surface sensitive (Palermo *et al*., 1998).

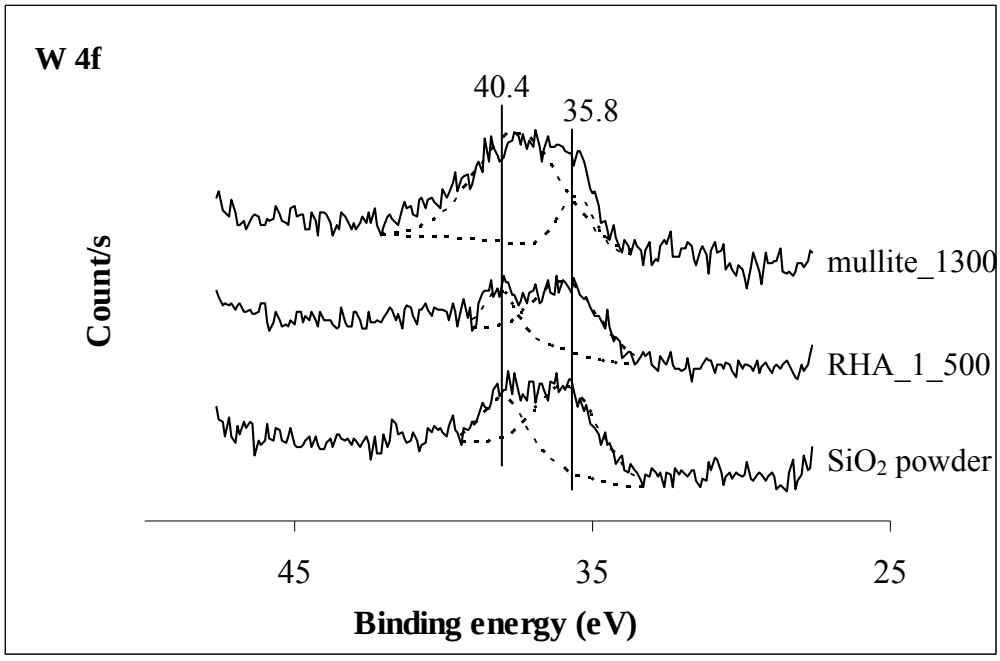

Figure 18 XPS spectra of W 4f region.

The XPS spectra of W 4f $_{5/2}$ and $4f_{7/2}$ in each catalyst was shown in Figure 18. The W $4f_{7/2}$ binding energy of each catalyst was observed of 35.8, 36.0 and 35.8 eV, respectively. The peak around 35.8 eV indicated the presence of W species as W^{6+}. The presence of Na on the surface would disperse and stabilize W species as WO_4^{2-} which was implicated as the OCM active site (Palermo *et al*., 1998). Another one peak of the each catalyst was shifted to 40.4, 40.5 and 39.9, respectively, which were attributed to W 4f $_{5/2}$.

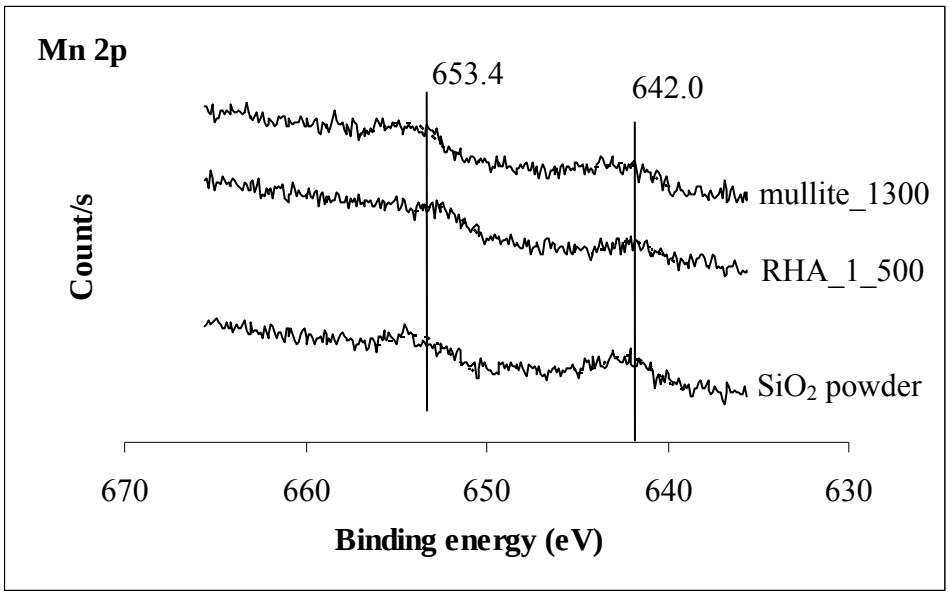

Figure 19 XPS spectra of Mn 2p region.

The XPS spectra of Mn $2p_{3/2}$ and $2p_{1/2}$ in each catalyst was shown in Figure 19. The Mn $2p_{3/2}$ binding energies were observed of 641.9 eV for Na_2WO_4-Mn/SiO_2 powder, 642.0 eV for Na_2WO_4-Mn/RHA_1_500, and 642.2 eV for Na_2WO_4-Mn/mullite_1300, indicating the presence of Mn^{3+} and Mn^{2+}, most likely in the form of Mn_2O_3 and $MnWO_4$ (Kou *et al*., 1998). These results were agreement with the characterization from XRD as shown in Figures 11 and 12. For the Mn $2p_{1/2}$, the binding energy of the synthesized catalyst was 653.4, 652.4 and 654.6 eV, respectively.

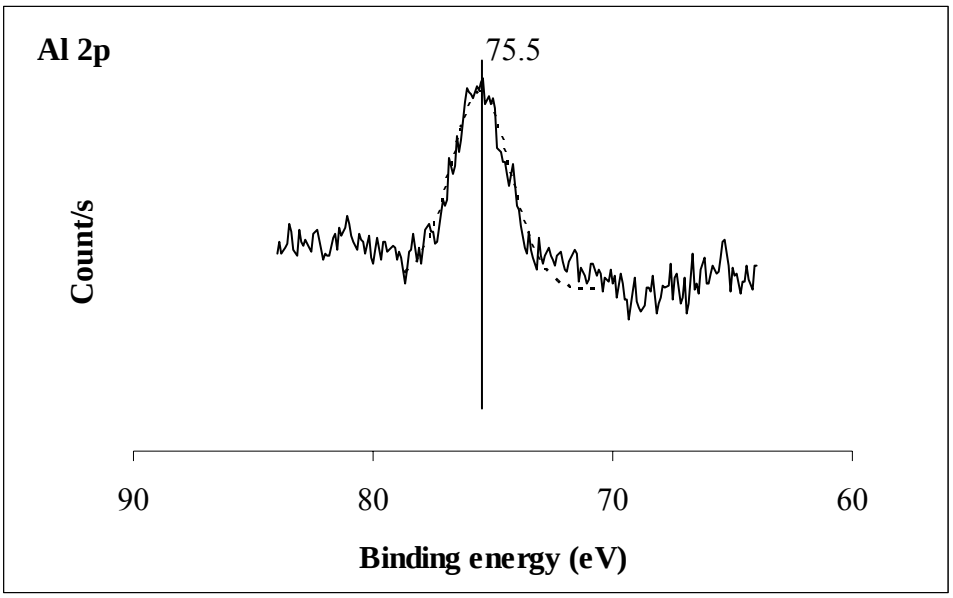

Figure 20 XPS spectra in the Al 2p region of Na_2WO_4-Mn/mullite_1300.

The XPS spectra in the Al 2p region and binding energy of Na_2WO_4-Mn/ mullite 1300ºC were shown in Figure 20. The Al 2p binding energy of a catalyst was observed at 75.5 eV, which was attributed to Al_2O_3.

From these XPS studies, the surface structure of the synthesized catalysts had been investigated. The surface structure of synthesized Na_2WO_4-Mn/SiO_2 was similar to the ones studied by Wang *et al*. (2005), and the synthesized Na_2WO_4-Mn/RHA_1_500. For Na_2WO_4-Mn/mullite_1300, the structures revealed the difference in the near-surface composition (at.%) of the species in the prepared catalysts of Na_2WO_4-Mn/SiO_2 powder, Na_2WO_4-Mn/RHA_1_500, and Na_2WO_4-Mn/mullite_1300 were shown in Table 10. Observations of the all species were emphasized on the Na 1s, W 4f, Mn 2p, Si 2p, Al 2p and O 1s core levels.

Table 10 Near-surface compositions (at.%) of Na_2WO_4-Mn catalyst on various supports

Catalyst supports	Na 1s	W 4f	Mn2p	Si 2p	Al 2p	O 1s		
						Al_2O_3	SiO_2	MO_x
SiO_2 powder	5.9	2.4	1.5	23.7			40.7	25.8
RHA_1_500	4.1	3.2	1.2	22.4			38.1	31.0
Mullite_1300	3.7	1.6	1.4	9.4	21.0	20.6	36.5	17.9

4. Catalytic activity test

From literature review (Kou *et al*., 1998 and Ji *et al*., 2002) the information from active group, the mechanism over Na_2WO_4-Mn can be written as following.

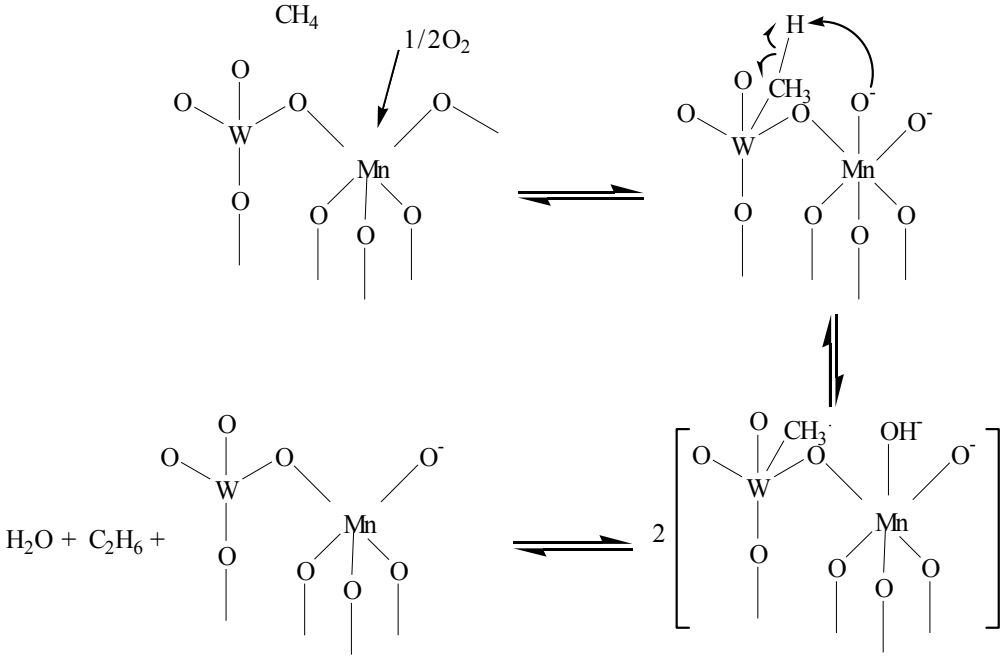

Figure 21 Proposed mechanism of OCM at the surface of Na_2WO_4-Mn catalyst.

The catalytic performances of the Na_2WO_4-Mn catalyst on various supports were investigated. The catalytic activity was studied at different OCM reaction temperatures with the CH_4/O_2/He volume ratio of 4/1/5 and flow rate 100 ml/min as shown in Figures 22-24.

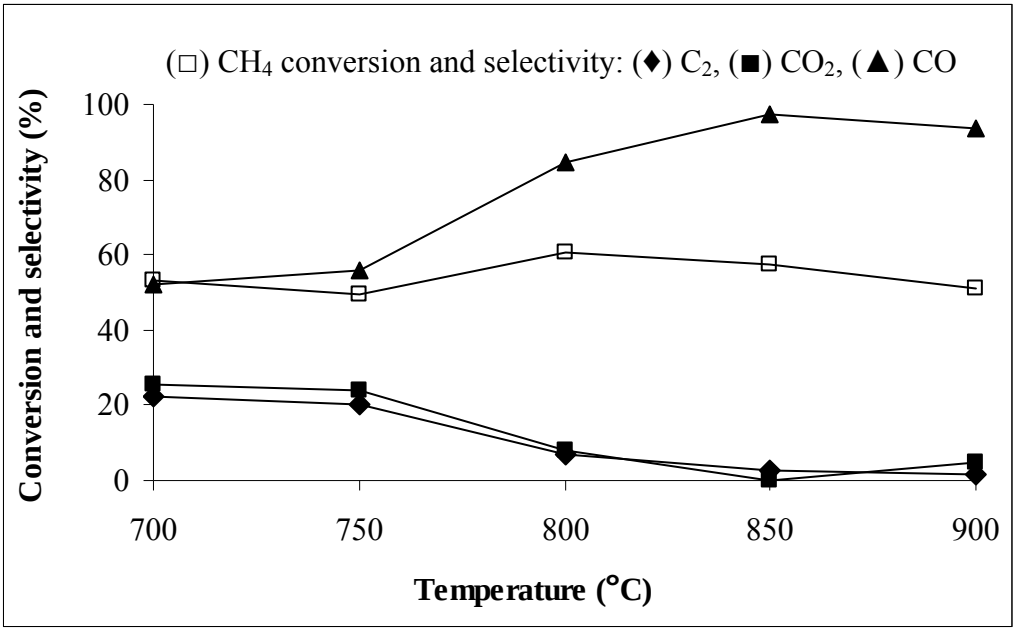

Figure 22 The catalytic performance at various temperatures of Na_2WO_4-Mn/SiO_2 powder.

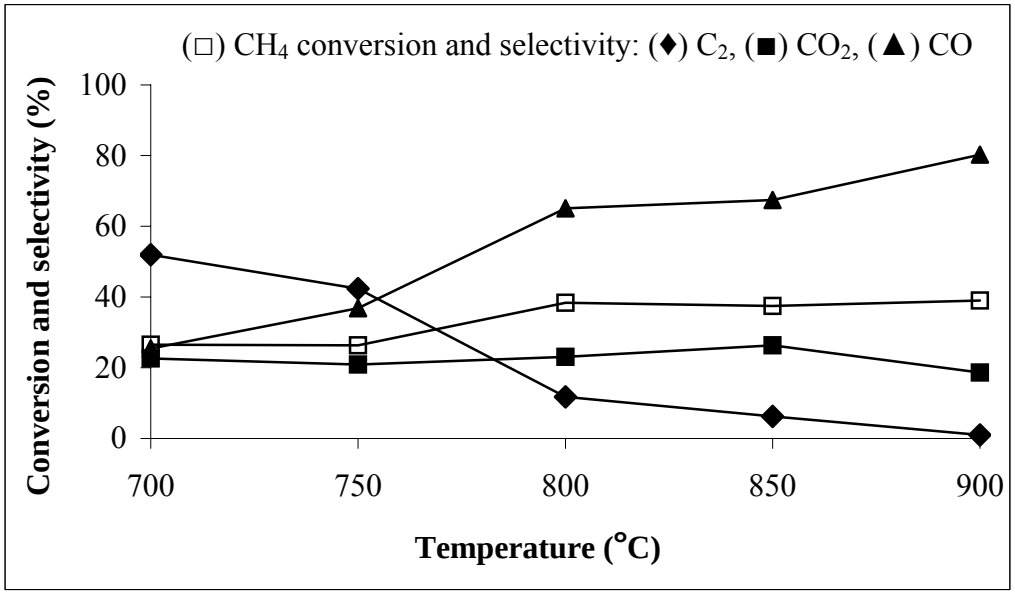

Figure 23 The catalytic performance at various temperatures of Na_2WO_4-Mn/ RHA_1_500.

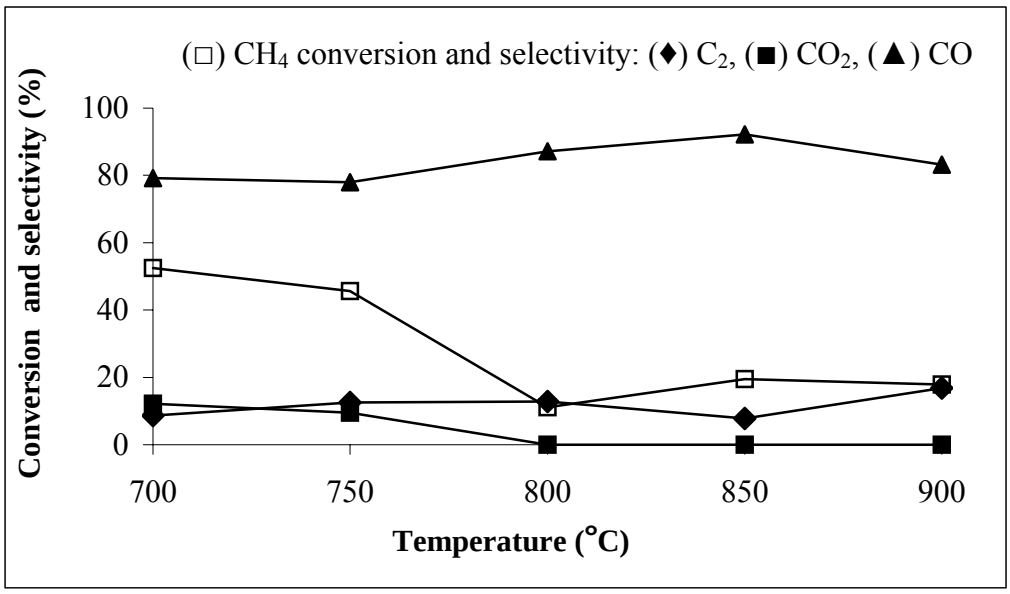

Figure 24 The catalytic performance at various temperatures of Na_2WO_4-Mn/ mullite_1300.

From Figures 22-24, the results showed methane conversion and products selectivity of all catalysts. With increasing in the reaction temperature from 700 to 800ºC, the conversion of methane slightly increased over Na_2WO_4-Mn/SiO_2 powder and Na_2WO_4-Mn/RHA_1_500. For Na_2WO_4-Mn/mullite_1300, methane conversion decreased with the increasing temperature from 700 to 800ºC, but no significant increase when increasing the reaction temperature from 800 to 900ºC. The best selectivity of C_2 hydrocarbon was occurred at 700ºC for Na_2WO_4-Mn/SiO_2 powder and Na_2WO_4-Mn/RHA_1_500 catalysts with 63.56 and 51.91%, respectively, and at 900ºC up to 16.78% for Na_2WO_4-Mn/mullite_1300. The CO_2 selectivity of Na_2WO_4-Mn/SiO_2 powder and Na_2WO_4-Mn/mullite_1300 was maximized at 25.54 and 12.14% at 700ºC and decreased with the increase in reaction temperature, where CO_2 selectivity of Na_2WO_4-Mn/RHA_1_500 was about 20% and slightly changed with the reaction temperature. For CO selectivity, Na_2WO_4-Mn/SiO_2 powder gave the increase in CO selectivity up to 97.35% at the temperature of 850ºC, where CO selectivity of Na_2WO_4-Mn/RHA_1_500 was maximized to 89.12% at 900ºC, whereas the increase was leveled off for Na_2WO_4-Mn/mullite_1300. A possible reason of the increase in CO selectivity with increasing reaction temperature was because the bulk

lattice oxygen more likely began to release, this facilitated the deep oxidation process of C_2 hydrocarbon. These results indicated the decrease in C_2 selectivity (Wang *et al*., 2005).

The catalytic performance of Na_2WO_4-Mn over various supports were reacted for OCM reaction at the reaction temperature of 800ºC, the CH_4/O_2/He volume ration of 4/1/5, and the flow rate of 100 ml/min as shown in Figures 25-32.

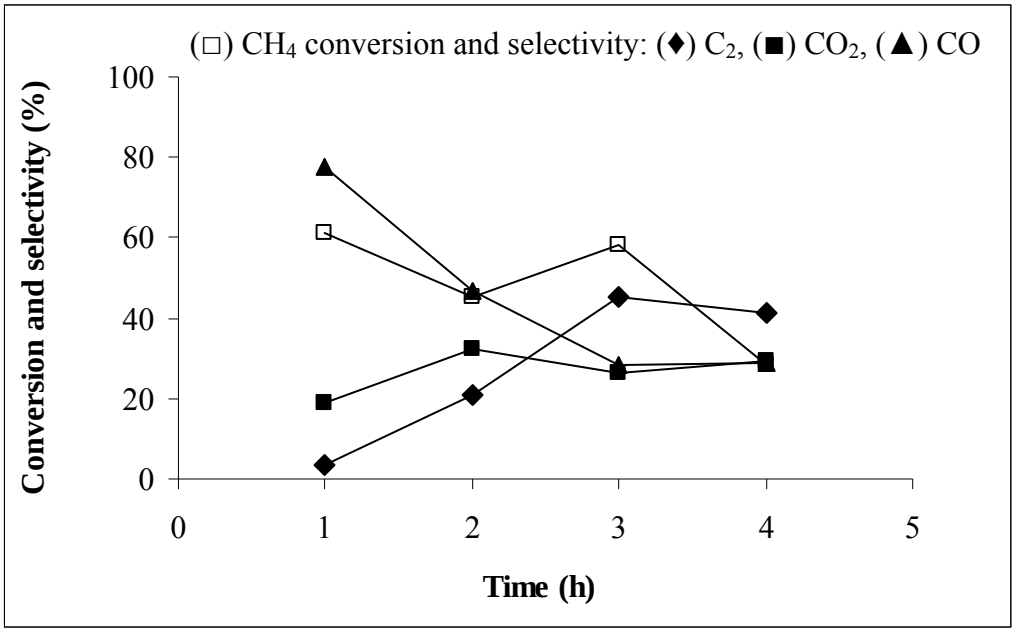

Figure 25 The catalytic performance of Na_2WO_4-Mn/SiO_2 powder.

Figure 25 showed the catalytic performance of Na_2WO_4-Mn/SiO_2 powder at 800ºC for 4 hours. The methane conversion was decreased from 46.23 to 26.99% with the increase reaction time. The CO_2 selectivity was maximized to 32.48% at 2 hours. For CO, the selectivity was decreased from 77.51 to 28.17%. The C_2 selectivity was increased from 3.62 to 45.45% with increasing the reaction time to 3 hours and decreased to 41.39% at 4 hours. The increase in C_2 selectivity was due to the active site of Na-O-W and Na-O-Mn in crystal phase of Na_2WO_4 and Mn_2O_3 induced the coupling of methyl radicals to C_2 hydrocarbon.

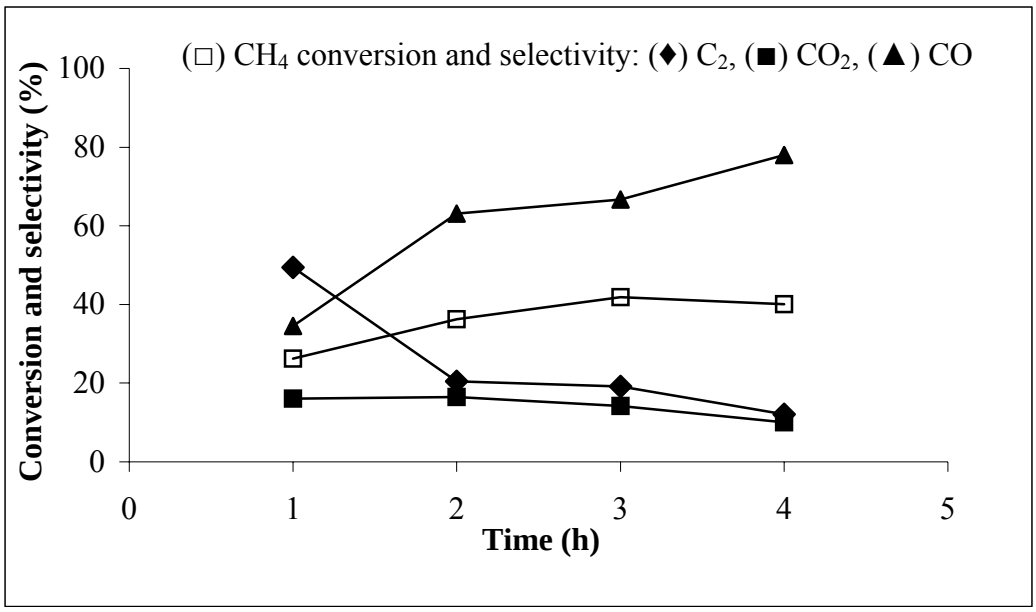

Figure 26 The catalytic performance of Na_2WO_4-Mn/RHA_1_500.

Figure 26 showed the catalytic performance of Na_2WO_4-Mn/RHA_1_500 at 800ºC for 4 hours. The methane conversion was increased from 26.24-41.89% with the increasing the times of reaction. CO_2 selectivity was slightly decreased from 16.43 to 9.99% while CO selectivity was increased from 34.55 to 77.99% with the increase in the reaction time. The C_2 selectivity was decreased from 49.40 to 12.02%; possible reasons of the fact that the decrease in the C_2 selectivity and the increase in CO selectivity were due to the reaction of methyl radical with lattice oxygen on surface which led to CO formation. Another reason could be the reaction of C_2 hydrocarbon with oxygen gas in gas phase of OCM reaction.

The catalytic performance of Na_2WO_4-Mn/RHA_1_900 at 800ºC for 4 hours was shown in Figure 27. The highest methane conversion was 40.48% in 1 hour, which was decreased to 33.40% in 4 hours. CO_2 selectivity was maximized to 29.88% in 1 hour. CO selectivity was increased from 60.09 to 83.56% in 3 hours and decreased to 66.54% in 4 hours. The C_2 selectivity was decreased from 10.04 to 5.65% in 3 hours and maximized to11.82% in 4 hours. The possible reason was also resulted from the reaction of methyl radical and C_2 hydrocarbon with oxygen gas.

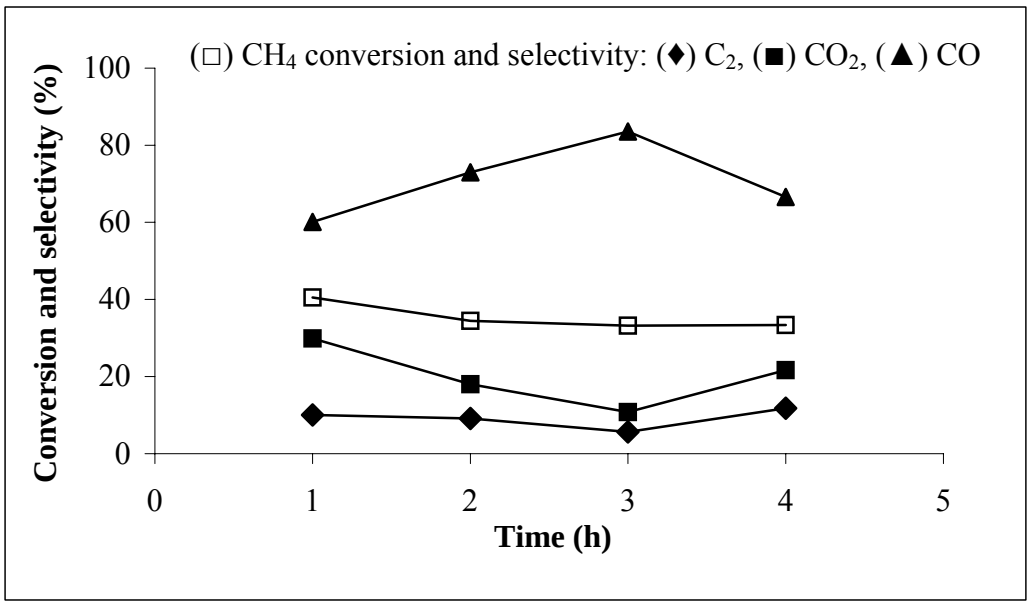

Figure 27 The catalytic performance of Na_2WO_4-Mn/RHA_1_900.

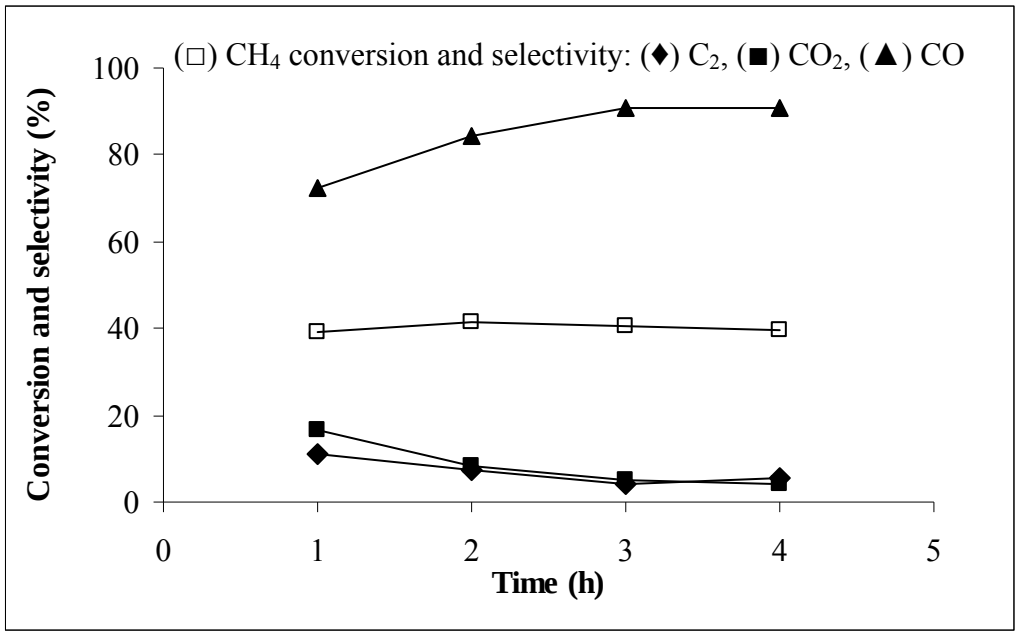

Figure 28 The catalytic performance of Na_2WO_4-Mn/RHA_3_900.

Figure 28 showed the catalytic performance of Na_2WO_4-Mn/RHA_3_900 at 800ºC for 4 hours. The best methane conversion was maximized to 41.62% in 2 hours. CO_2 selectivity was decreased from 16.47 to 3.95%. CO selectivity was maximized to 90.82% in 3 hours. The C_2 selectivity was maximized to 11.26% in 1 hour. The decrease in the C_2 selectivity and the increase in CO selectivity were due to the reaction of methyl radical with lattice oxygen on surface leding CO formation.

The catalytic performance of Na_2WO_4-Mn/mullite_1200 at 800ºC was shown in Figure 29. The methane conversion decreased from 37.24 to 14.81% in 3 hours. The CO_2 and CO selectivity were about 8 and 88%, respectively, and no significant change with the reaction time. C_2 selectivity was about 3% without significant changed with the reaction time; possible reason for the low C_2 selectivity and the high CO selectivity was the transformation of Na_2WO_4 and Mn_2O_3 to $MnWO_4$ (equation 20). The absence of active site indicated that the methane radical was easily reacted with the O_s^- on surface catalysts to CO formation.

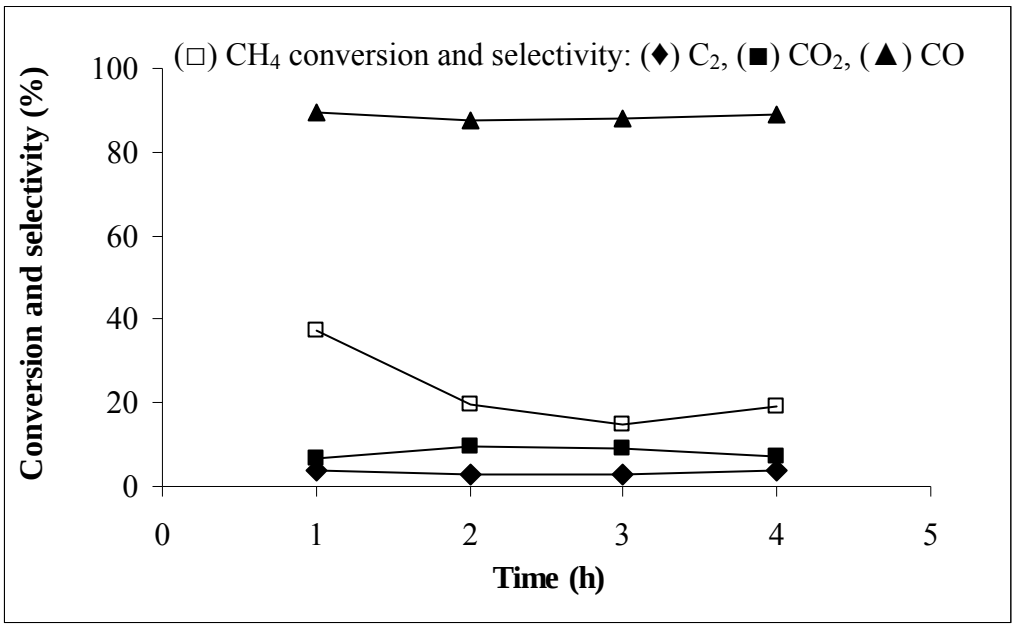

Figure 29 The catalytic performance of Na_2WO_4-Mn/mullite_1200.

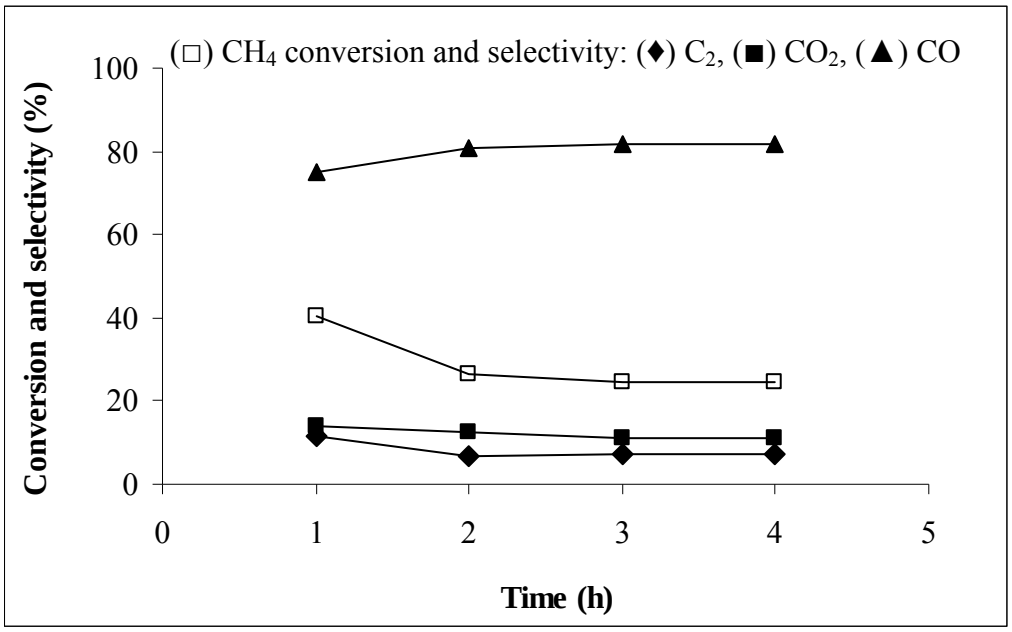

Figure 30 The catalytic performance of Na_2WO_4-Mn/mullite_1300.

Figure 30 showed the catalytic performance of Na_2WO_4-Mn/mullite_1300 at 800ºC for 4 hours. The methane conversion was slightly decreased from 40.39 to 26.36% in 2 hours then became consistent. CO_2 selectivity was slightly decreased from 13.76 to 10.99%. CO selectivity was slightly increased from 74.89 to 81.97%. C_2 selectivity obtained the low value in the range of 6.95-11.35% and the best selectivity was 11.35% at 1 hour. A possible reason for the low C_2 selectivity and the high CO selectivity were observed due to the methane radical was easily reacted with the O_s^- on surface catalysts to CO formation.

The catalytic performance of Na_2WO_4-Mn/mullite_1400 at 800ºC for 4 hours was shown in Figure 31. The methane conversion was slightly decreased from 56.65 to 46.19% in 2 hours then became consistent. CO_2 selectivity was about 13% without significant change with the reaction time. CO selectivity was slightly increased from 79.59 to 83.67% in 4 hours. C_2 selectivity was about 5% without significant change with the reaction time. A possible reason of the low C_2 selectivity and the high CO

selectivity was due to the fact that the methane radical was easily reacted with the O_s^- on surface catalysts to CO formation.

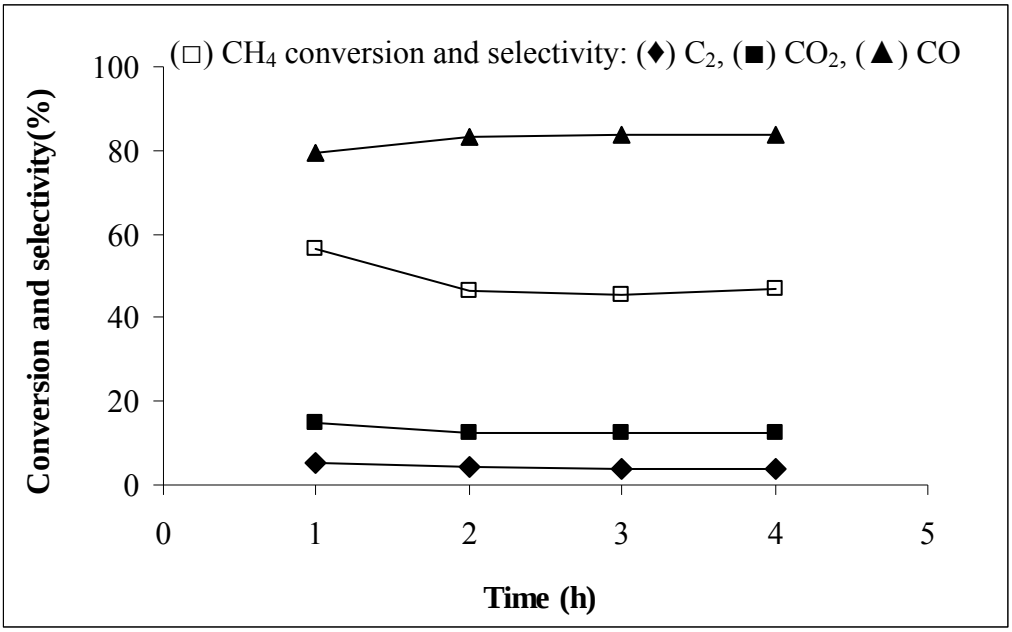

Figure 31 The catalytic performance of Na_2WO_4-Mn/mullite_1400.

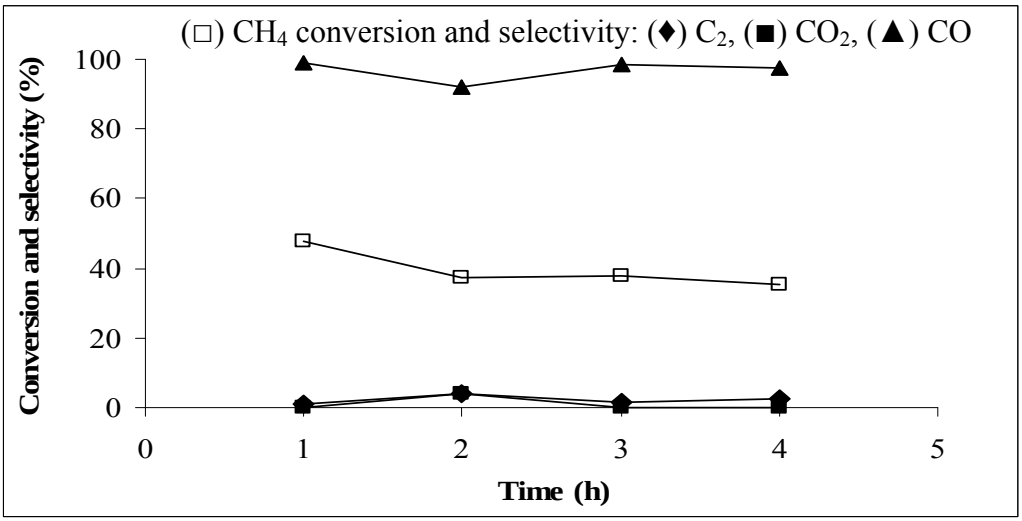

Figure 32 The catalytic performance of Na_2WO_4-Mn/mullite_1500.

Figure 32 showed the catalytic performance of Na_2WO_4-Mn/mullite_1500 at 800ºC for 4 hours. The methane conversion was maximized at 47.79% in 1 hour. CO_2 selectivity was maximized at 4.01% in 2 hours. CO selectivity was maximized of 99.10% in 1 hour. C_2 selectivity was maximized of 3.78% in 2 hours. A possible reason for the low C_2 selectivity and the high CO selectivity was also from the reaction of the methyl radical and the O_s^- on surface catalyst to CO formation.

The maximum conversion and selectivity of C_2, CO_2 and CO at different temperature and reaction time on different supports could be summarized as shown in Tables 11 and 12.

Table 11 The reaction temperature to achieve the maximum conversion and selectivity of C_2, CO_2 and CO on Na_2WO_4-Mn on different supports

Catalyst supports	CH_4 conversion (%)	Selectivity (%)		
		C_2	CO_2	CO
SiO_2 powder	60.75 (800)*	22.18 (700)	25.54 (700)	97.35 (900)
RHA_1_500	38.39 (800)	51.91 (700)	26.38 (850)	89.12 (900)
mullite_1300	52.49 (700)	16.78 (900)	12.14 (700)	92.23 (850)

* (Reaction temperature, ºC)

For the OCM reaction to C_2 hydrocarbon, Na_2WO_4-Mn/RHA_1_500 was the appropriate catalyst due to the highest C_2 selectivity of 51.91% at 700ºC, which was higher than the C_2 selectivity on Na_2WO_4-Mn on SiO_2 powder and mullite_1300. However, Na_2WO_4-Mn/RHA_1_500 had the low CH_4 conversion of 38.39 % at 800ºC compared to the one on SiO_2 powder with 60.75% at 800ºC. In the CO application, Na_2WO_4-Mn/SiO_2 powder could produce CO with the selectivity of 97.35% at 900ºC. For Na_2WO_4-Mn/mullite, the CH_4 conversion was at 52.49% at 700ºC with the lowest C_2 selectivity of 16.78 % at 900ºC.

Table 12 The reaction time to achieve the maximum conversion and selectivity of C_2, CO_2 and CO on Na_2WO_4-Mn on different supports at 800ºC

Catalyst supports	CH_4 conversion (%)	Selectivity (%)		
		C_2	CO_2	CO
SiO_2 powder	61.09 (1)*	45.45 (3)	32.48 (2)	77.51 (1)
RHA_1_500	41.89 (3)	49.40 (1)	16.43 (2)	77.99 (4)
RHA_1_900	40.48 (1)	11.82 (4)	29.88 (1)	83.56 (3)
RHA_3_900	41.62 (2)	11.26 (1)	16.47 (1)	90.82 (3)
mullite_1200	37.24 (1)	3.79 (4)	9.65 (2)	89.59 (1)
mullite_1300	40.39 (1)	11.35 (1)	13.76 (1)	81.97 (3)
mullite_1400	56.65 (1)	5.50 (1)	14.91 (1)	83.67 (4)
mullite_1500	47.79 (1)	3.78 (2)	4.01 (2)	99.10 (1)

* (hours)

From the comparison among mullites at various sintering temperatures, Na_2WO_4-Mn/mullite_1400 gave the highest CH_4 conversion of 56.65% but the lowest C_2 selectivity of 5.50% at 1 hour of reaction, whereas Na_2WO_4-Mn/mullite_1300 gave the highest C_2 selectivity of 11.35% and CH_4 conversion of 40.39% in 1 hour. Among Na_2WO_4-Mn supported on RHA catalysts, Na_2WO_4-Mn/RHA_1_500 gave the highest C_2 selectivity of 49.40% and CH_4 conversion of 41.89% in 1-3 hours of reaction. Among three various supported Na_2WO_4-Mn catalysts, Na_2WO_4-Mn/SiO_2 powder gave the highest CH_4 conversion of 61.09% and moderately C_2 selectivity of 45.45%, slightly less than the highest C_2 selectivity of 49.40% from Na_2WO_4-Mn/RHA_1_500. This information could lead to the appropriate condition in OCM operation in order to maximize conversion and selectivity.

4. Catalyst stability

To study the stability of the fresh and after 4 h used catalysts, Na_2WO_4-Mn over SiO_2 powder, RHA_1_500 and mullite_1300 were characterized by XRD as shown in Figures 33-35.

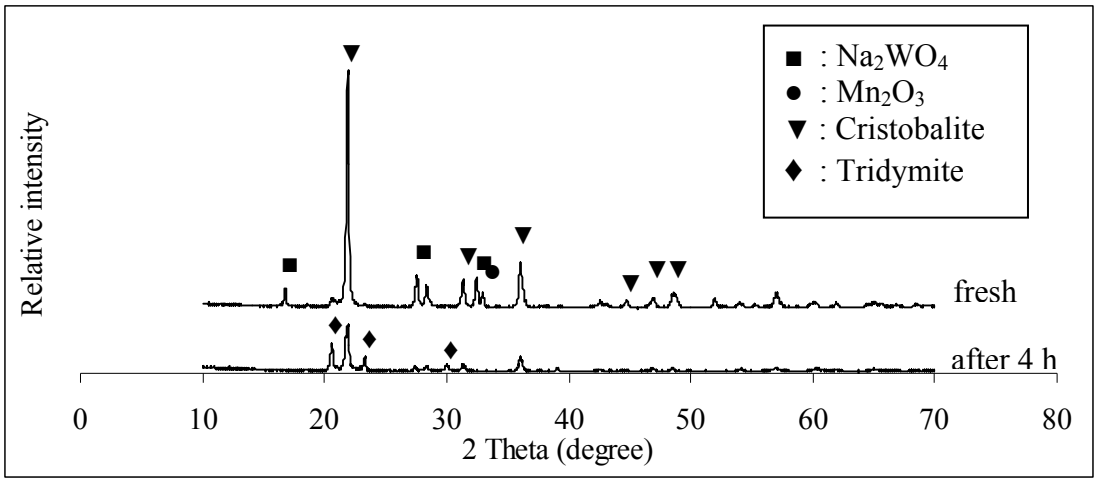

Figure 33 The XRD patterns of Na_2WO_4-Mn/SiO_2 powder catalyst.

In Figure 33, the XRD patterns of the after 4 hours used Na_2WO_4-Mn/SiO_2 powder catalyst showed that the supported SiO_2 phase was transformed from cristobalite into tridymite and the crystal phases of Na_2WO_4 and Mn_2O_3 were disappeared.

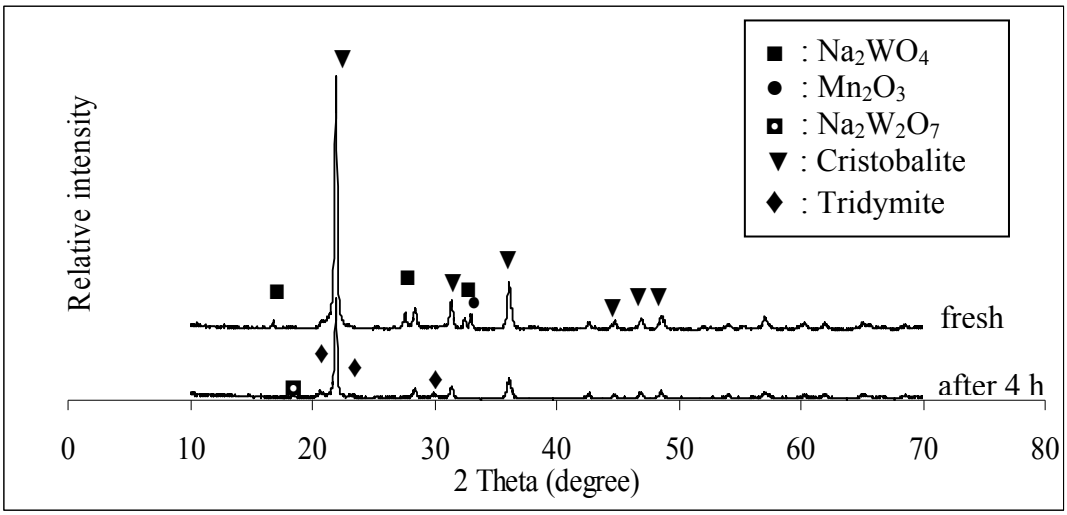

Figure 34 The XRD patterns of Na_2WO_4-Mn/RHA_1_500 catalyst.

Compare to after 4 hours used Na_2WO_4-Mn/RHA_1_500 in Figure 34, the XRD pattern showed the transformation of cristobalite to tridymite phase. The crystal phase of Na_2WO_4 was transformed to $Na_2W_2O_7$, respectively, which $Na_2W_2O_7$ was found to be active in OCM reaction (Ji *et al*., 2002).

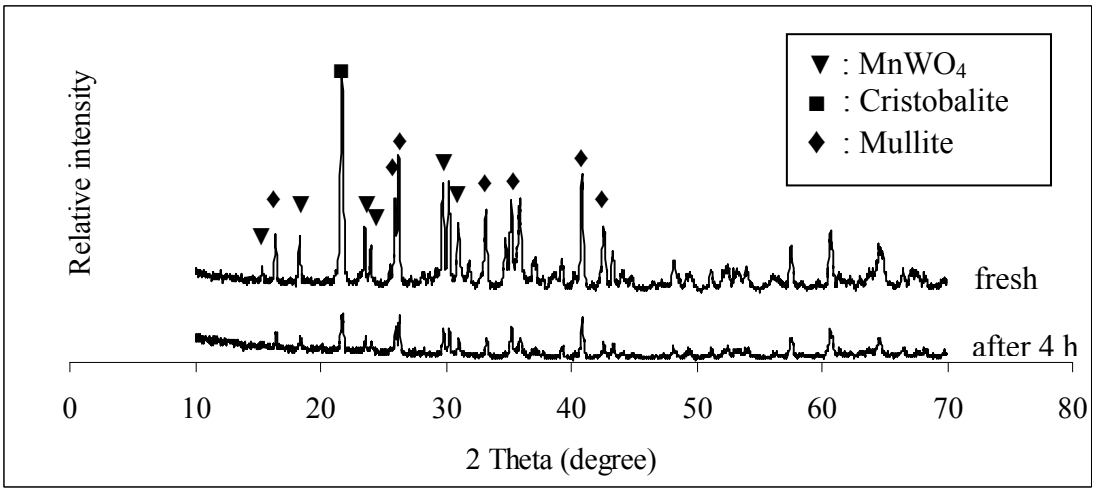

Figure 35 The XRD patterns of Na_2WO_4-Mn/mullite_1300 catalyst.

For Na_2WO_4-Mn/mullite sinterd at1300°C after 4 h use in OCM reaction, the metal oxide of $MnWO_4$ still remained on the surface.

CONCLUSION

The Na_2WO_4-Mn catalysts supported on silica powder, rice husk ash and mullite were prepared by the incipient wetness impregnation method. From XRD characterization, the structures of supports were amorphous for silica powder, semi-crystalline, quartz and cristobalite for rice husk ash, and for mullite, the structures were crystalline mullite contaminated with cristobalite and corundum. For the crystalline phases of metal oxide, there were Na_2WO_4 and Mn_2O_3 on Na_2WO_4-Mn/SiO_2 powder and Na_2WO_4-Mn/RHA_1_500, Na_2WO_4, Mn_2O_3 and $MnWO_4$ on Na_2WO_4-Mn/RHA_1_900 and Na_2WO_4-Mn/RHA_3_900, and $MnWO_4$ on Na_2WO_4-Mn/ mullite. From XPS studies, the results revealed the information on Na, W and Mn species distributed on the catalyst surface, which agreed with the information from XRD. By looking at the specific surface area of the supports and the prepared catalysts, the specific surface area of rice husk ash and mullite supports were decreased with increasing the calcination temperature. The specific surface area of Na_2WO_4-Mn/silica powder and Na_2WO_4-Mn/rice husk ash were dramatically decreased due to the transformation of amorphous silica to cristobalite. The specific surface area of Na_2WO_4-Mn supported on sintered mullites at 1200 and 1300ºC was decreased due to the pore filling by metal oxide. For Na_2WO_4-Mn supported on sintered mullite at 1400 and 1500ºC, the surface area was increased because of metal oxide aggregates on the dense surface.

To study the catalytic activity of catalysts at different reaction time and temperatures, Na_2WO_4-Mn/SiO_2 powder gave the highest CH_4 conversion of around 61% at the temperature of 800ºC in 1 hour and as high as 45% C_2 selectivity in 3 hours. By looking at XRD of fresh and 4 h used Na_2WO_4-Mn/SiO_2 powder, there was no Na_2WO_4 and Mn_2O_3 remained on the 4 h used one, the results was also happened on Na_2WO_4-Mn/RHA after 4 h use. For Na_2WO_4-Mn/RHA, the highest CH_4 conversion at 800ºC was around 39-42% with its C_2 selectivity up to 52%; its structure after 4 h use was $Na_2W_2O_7$ which was active in OCM reaction. Moreover, C_2 selectivity on SiO_2 powder and RHA supports was increased with the increase of

Na_2WO_4 crystal size. For Na_2WO_4-Mn/mullite, the highest CH_4 conversion at 800ºC was around 57% and its C_2 selectivity of 23%; its structure after 4 h use was relatively similar to the fresh one.

These results revealed that although Na_2WO_4-Mn/SiO_2 powder gave the highest CH_4 conversion and good selectivity, the catalyst was unstable for long time use. However, for the support of mullite and RHA, these catalysts gave good conversion but fair C_2 selectivity, its structure after 4 h use implied that the catalyst could be reused. There could be more studies to improve Na_2WO_4-Mn/SiO_2 powder and Na_2WO_4-Mn/RHA to be more stable and for longer use.

.

LITERATURE CITED

Au, C. T., Y. W. Liu, and C. F. Ng. 1998. Raman spectroscopic and TPR studies of oxygen species over BaO and BaX_2(X = F, Cl, Br)-promoted Nd_2O_3 Catalysts for the oxidative coupling of methane. **J. Catal.** 176: 365-375.

Barea, R., M. I. Osendi, J. M. F. Ferreira and P. Miranzo. 2005. Thermal conductivity of highly porous mullite material. **Act. Mater.** 53: 3313-3318.

Bond, G. C. 1987. **Heterogeneous Catalysis: Principles and Application**. Clarendon Press, Oxford, UK.

_____. 1989. **Catalysis 8**. Royal Society of Chemistry, Cambridge, UK.

Boonpa, S. 2006. **Mullite Synthesis by Aluminum Hydroxide and Silica from Rice Husk Ash.** M.S. Thesis, Kasetsart University.

Chang, F., W. Kuo and H. Yang. 2005. Preparation of Cr_2O_3-promoted copper catalysts on rice husk ash by incipient wetness impregnation. **App. Catal. A.** 288: 53-61.

Chakraborty, A. K. 2005. Aluminosilicate formation in various mixtures of tetra ethyl orthosilicate (TEOS) and aluminium nitrate (ANN). **Therm. Act.** 427: 109-116.

Chou, L., Y. Cai, B. Zhang, J. Nio, S. Ji and S. Li. 2003. Influence of SnO_2-doped W-Mn/SiO_2 for oxidative coupling of methane to high hydrocarbons at elevated pressure. **Appl. Catal. A.** 238: 185-191.

Della,V. P., I. Kuhn and D. Hotza. 2001. Rice husk ash as an alternate source for active silica production. **Mater. Lett.** 57: 818-821.

Ertl, G., H. Knozinger and J.Weitkamp, eds. 1997. Handbook of heterogeneous **Catalyst.** Vol. 4. Wiley-VCH, Weinheim.

Faith, W. L., D. B. Keyes, and R. L. Clark. 1957. Industrial Chemicals. John Wiley & Sons.

Feng, Q., H. Yamamichi, M. Shoya and S. Sugita. 2004. Study on the pozzolanic properties of rice husk ash by hydrochloric acid pretreatment. **Cem. Concr. Res.** 34: 521-526.

Gong, M. C., X. H. Xu, Y. Q. Chen, J. L. Zhou and Y. Chen. 1995. Study on oxidative coupling of methane. Effect of additives on TiO_2-based catalytic performance. **Catal. Today.** 24: 263-264.

Guha, K and J. Roy. 1988. Gas chromatography grade silica gel from paddy husk ash. **J. Chromatography.** 473: 245-248.

He, Y., B. Yang and G. Cheng. 2004. On the oxidative coupling of methane with carbon dioxide over CeO_2/ZnO nanocatalysts. **Catal. Today.** 98: 595-600.

Hou, S., Y. Cao, W. Xiong, H. Liu and Y. Kou. 2006. Site requirement for the oxidative coupling of methane on SiO_2-supported Mn catalysts. **Ind. Eng. Chem. Res.** 45: 7077-7083.

Huang, S., S. Jing, J. Wang, Z. Wang and Y. Jin. 2001. Silica white obtained from rice husk in a fluidized bed. **Powder Technology**. 117: 232-238.

Ji, S., S. Li, Y. Liu, L. Gao, J. Niu and C. Xu. 1999. Rule of sodium in the oxidative coupling of methane over Na-W-Mn/SiO_2 catalysts. **J. Nat. Gas. Chem.** 8: 1-8.

_____, T. Xiao, S. Li, C. Xu, R. H, K. S. Coleman and M. L. H. Green. 2002. The relationship between the structure and the performance of Na-W-Mn/ SiO_2 catalysts for oxidative coupling of methane. **Appl. Catal. A.** 225: 271-284.

_____, _____, S. Li, L. Chou, B. Zhang, C. Xu, R. Hou, A. P. E. York and M. L. H. Green. 2003. Surface WO_4 tetrahedron: the essence of the oxidative coupling of methane over Na-W-Mn/ SiO_2 catalysts. **J. Catal.** 220: 47-56.

Jiang, Z., C. Yu, X Fang, S. Li and H. Wang. 1993. Oxide/support interaction and surface reconstruction in the Na_2WO_4/SiO_2 system. **J. Phys. Chem.** 97: 12870-12875.

Kalapathy, U., A. Proctor and J. Shultz. 2000. A simple method for production of pure silica from rice hull ash. **Biores. Technol.** 73: 257-262.

_____, _____ and _____. 2002. An improved method for production of silica from rice hull ash. **Biores. Technol.** 85: 285-289.

Kondratenko, E.V., N. G. Maksimov, G. E. Selyutin and A.G. Anshits. 1995. Oxidative coupling of methane over oxides of alkali earth metals using N_2O as oxidant. **Catal. Today.** 24: 273-275.

Kus, S., M. Otremba and M. Taniewski. 2003. The catalytic performance in oxidative coupling of methane and the surface basicity of La_2O_3, Nd_2O_3, ZrO_2 and Nb_2O_5. **Fuel.** 82: 1331-1338.

Kou, Y., B. Zhang, J. Niu, S. Li, H. Wang, T. Tanaka and S. Yoshida. 1998. Amorphous features of working catalysts: XAFS and XPS characterization of $Mn/Na_2WO_4/SiO_2$ as used for the oxidative coupling of methane. **J. Catal.** 173: 399-408.

Li, S. 2003. Reaction chemistry of W-Mn/SiO_2 catalyst for the oxidative coupling of methane. **J. Natural Gas Chemistry.** 12: 1-9.

Lin, C. H., J. X. Wang and J. H. Lunsford. 1988. Oxidative dimerization of methane over sodium-promoted calcium oxide. **J. Catal.** 111: 302-316.

Lunsford, J. H. 1995. The catalytic oxidative coupling of methane. **Angew. Chem. Int. Ed. Engl.** 34: 970-980.

_____. 2000. Catalytic conversion of methane to more useful chemicals and fuels: a challenge for the 21st century. **Catal. Today.** 63: 165-174.

Montes, O. B., M. I. Nieto and R. Moreno. 2007. Mullite compacts obtained by colloidal filtration of alumina powders dispersed in colloidal silica suspensions. **Ceram. Int.** 33: 327-332.

Moore, J. W., W. G. Davies and R. W. Collis. 1978. **Chemistry.** Kogakusha McGraw-hill, Japan.

Murata, K., T. Hayakawa, S. Hamakawa and K. Suzuki. 1998. Lithium-doped sulfated-zirconia catalysts for oxidative coupling of methane to give ethylene and ethane. **Catal. Today.** 45: 41-45.

Otsuka, K., I. Yamanaka and Y. Wang. 1998. Reductive activation of oxygen for partial oxidation of light alkanes. **Stud. Surf. Sci.** 119: 15-24.

Pak, S. and J. H. Lunsford. 1998. Thermal effects during the oxidative coupling of methane over Mn/Na_2WO_4/SiO_2 and Mn/Na_2WO_4/MgO catalysts. **Appl. Catal. A** 168: 131-137.

Park, Y. M., T. Y. Yang, S. Y. Yoon, R. Stevens and H.C. Park. 2007. Mullite whiskers derived from coal fly ash. **Mater. Sci. Eng. A** 454-455: 518-522.

Palermo, A., J. P. H. Vazquez, A. F. Lee, M. S. Tikhov and R. M. Lambert. 1998. Critical influence of the amorphous silica-to-cristobalite phase transition on the performance of $Mn/Na_2WO_4/SiO_2$ catalysts for the oxidative coupling of methane. **J. Catal.** 177: 259-266.

Patterson, A. L. 1939. The scherrer formula for x-ray particle size determination. **Phy. Rev.** 56: 978-982.

Ribeiro, M. J., D. U. Tulyaganov, J. M. F. Ferreira and J. A. Labrincha. 2004. Production of Al-rich sludge-containing ceramic bodies by different shaping techniques. **J. Mater. Process. Technol.** 148: 139-146.

_____, _____, _____ and _____. 2005. High temperature mullite dissolution in ceramic bodies derived from Al-rich sludge. **J. Euro. Ceram. Soc.** 25: 703–710.

Shinohara, Y. and Kohyama, N. 2004. Quantitative analysis of tridymite and cristobalite crystallized in rice husk ash by heating. **Industrial Health.** 42: 277-285.

She, J.H. and T. Ohji. 2003. Fabrication and characterization of highly porous mullite caramics. **Mat. Chem. Phy.** 80: 610-614.

Schneider, H., K. Okada and J. A. Pask. 1994. **Mullite and Mullite Ceramics.** John Wiley & Sons, New York, USA.

Taniewski, M., A. Lachowicz, K. Skutil and D. Czechowicz. 1996. The effect of dilution of the catalyst bed on its heat-transfer characteristics in oxidative coupling of methane. **Chem. Eng. Sci.** 51: 4271-4278.

Traykova, M., N. Davidova, J.-S. Tsaih and A. H. Weiss. 1998. Oxidative coupling of methane - the transition from reaction to transport control over La_2O_3/MgO catalyst. **J. Appl. Catal. A.** 169**:** 237-247.

Tsay, M and F. Chang. 2001. Characterization and reactivity of RHA-Al_2O_3 composite oxide supported nikel catalysts. **Catal. Commun.** 2: 233-239.

Vieira, S. C., A. S. Ramos and M.T. Vieira. 2007. Mullitization kinetics from silica- and alumina-rich wastes. **Ceram. Int.** 33: 59-66.

Wang, D., M. P. Rosynek and J. H. Lunsford. 1995. Oxidative coupling of methane over oxide-supported sodium- manganese catalysts. **J. Catal.** 155: 390-402.

Wang, J., L. Chou, B. Zhang, H. Song, J. Zhao, J. Yang and S. Li. 2005. Comparative study on oxidation of methane to ethane and ethylene over Na_2WO_4-Mn/SiO_2 Catalysts prepared by different method. **J. Mol. Catal. A** 245: 272-277.

_____, _____, _____, _____, _____, _____ and _____. 2006. Low-temperature selective oxidation of methane to ethane and ethylene over $BaCO_3/La_2O_3$ catalysts prepared by urea combustion method. **Catal. Commu.** 7: 59-63.

Yamamura, M., H. Okado, N. Tsuzuki, T. Wakatsuki and K. Otsuka. 1995. Oxidative coupling of methane over ternary metal oxide catalysts consisting of groups I, III, and V elements in the periodic table. **Appl. Catal. A.** 122: 135-149.

Yalcin, N., and V. Sevinc. 2001. Studies on silica obtained from rice husk. **Ceram. Int.** 27: 219-224.

Zhang, H., J. Wu, B. Xu and C. Hu. 2006a. Simultaneous production of syngas and ethylene from methane by combining its catalytic oxidative coupling over $Mn/Na_2WO_4/SiO_2$ with gas phase partial oxidation. **Catal. Lett.** 106: 161-165.

_____, _____, S. Qin and C. Hu. 2006b. Study of the gas space time on the combination of methane gas-phase oxidation and catalytic oxidative coupling over $Mn/Na_2WO_4/SiO_2$ catalyst. **Ind. Eng. Chem. Res.** 45: 7090-7095.